Cell Calcium 84 (2019) 102080

Contents lists available at ScienceDirect

Cell Calcium

journal homepage: www.elsevier.com/locate/ceca

Pseudomonas aeruginosa β-carbonic anhydrase, psCA1, is required for calcium deposition and contributes to virulence

Shalaka R. Lotlikar[a,1], Biraj B. Kayastha[a,1], Daniela Vullo[b], Sharmily S. Khanam[a], Reygan E. Braga[a], Akilah B. Murray[c], Robert McKenna[c], Claudiu T. Supuran[d], Marianna A. Patrauchan[a,*]

[a] Department of Microbiology and Molecular Genetics, Oklahoma State University, Stillwater, OK 74078, USA
[b] Università degli Studi di Firenze, Polo Scientifico, Laboratorio di Chimica Bioinorganica, Rm. 188, Via della Lastruccia 3, 50019 Sesto Fiorentino, Florence, Italy
[c] Department of Biochemistry and Molecular Biology, College of Medicine, University of Florida, Gainesville, FL 32610, USA
[d] Università degli Studi di Firenze, Polo Scientifico, Dipartimento Neurofarba, Sezione di Scienze Farmaceutiche, Via Ugo Schiff 6, 50019 Sesto Fiorentino, Florence, Italy

ARTICLE INFO

Keywords:
Carbonic anhydrases
Calcium carbonate
Gene-deletion mutants
Transmission electron microscopy
qRT-PCR

ABSTRACT

Calcification of soft tissue leads to serious diseases and has been associated with bacterial chronic infections. However, the origin and the molecular mechanisms of calcification remain unclear. Here we hypothesized that a human pathogen *Pseudomonas aeruginosa* deposits extracellular calcium, a process requiring carbonic anhydrases (CAs). Transmission electron microscopy confirmed the formation of 0.1-0.2 μm deposits by *P. aeruginosa* PAO1 growing at 5 mM $CaCl_2$, and X-ray elemental analysis confirmed they contain calcium. Quantitative analysis of deposited calcium showed that PAO1 deposits 0.35 and 0.75 mM calcium/mg protein when grown at 5 mM and 10 mM $CaCl_2$, correspondingly. Fluorescent microscopy indicated that deposition initiates at the cell surface. We have previously characterized three PAO1 β-class CAs: psCA1, psCA2, and psCA3 that hydrate CO_2 to HCO_3^-, among which psCA1 showed the highest catalytic activity (Lotlikar et. al. 2013). According to immunoblot and RT-qPCR, growth at elevated calcium levels increases the expression of *psCA1*. Analyses of the deletion mutants lacking one, two or all three *psCA* genes, determined that *psCA1* plays a major role in calcium deposition and contributes to the pathogen's virulence. *In-silico* modeling of the PAO1 β-class CAs identified four amino acids that differ in psCA1 compared to psCA2, and psCA3 (T59, A61A, A101, and A108), and these differences may play a role in catalytic rate and thus calcium deposition. A series of inhibitors were tested against the recombinant psCA1, among which aminobenzene sulfonamide (ABS) and acetazolamide (AAZ), which inhibited psCA1 catalytic activity with K_{Is} of 19 nM and 37 nM, correspondingly. The addition of ABS and AAZ to growing PAO1 reduced calcium deposition by 41 and 78, respectively. Hence, for the first time, we showed that the β-CA psCA1 in *P. aeruginosa* contributes to virulence likely by enabling calcium salt deposition, which can be partially controlled by inhibiting its catalytic activity.

1. Introduction

Soft tissue calcification is highly disruptive for cellular functions and leads to severe human diseases such as arteriosclerosis and renal stone formations. However, the origins and the contributing factors of calcification are poorly understood. Initiation of calcification is commonly associated with misbalance of calcium ion (Ca^{2+}) and activity of human alkaline phosphatases and carbonic anhydrases (CAs) [1,2]. Several diseases lead to elevated levels of Ca^{2+} in different liquids of the human body. For example, the levels of Ca^{2+} are increased in pulmonary fluids and nasal secretions in cystic fibrosis (CF) patients [3,4], in serum of patients with cardiovascular disease (CVD) and hypertension [5,6], during arteriosclerosis [7], and chronic kidney disease [8]. Furthermore, scattered calcium salt deposits have been observed in calcified atherosclerotic lesions of endocarditis patients [9]. Calcium deposition was also detected during late stages of long-term chronic bacterial infections, such as CF, tuberculosis and infective endocarditis [10–12]. The latter raises a possibility that bacterial pathogens may contribute to the process of calcium deposition in soft tissues of the host. This concept has been previously proposed in the context of

* Corresponding author.
E-mail address: m.patrauchan@okstate.edu (M.A. Patrauchan).
[1] The authors contributed equally.

https://doi.org/10.1016/j.ceca.2019.102080
Received 4 April 2019; Received in revised form 16 August 2019; Accepted 7 September 2019
Available online 27 September 2019

Table 1
Bacterial strains and plasmids used in this study.

Strain/plasmid	Relevant Characteristics	Source
Escherichia coli		
E. coli DH5α	General purpose cloning strain; *Δ(lacZ)M15)*	New England Biolabs
ECOlot1	*E. coli* DH5α harboring plasmid pLOT1	This study
ECOlot2	*E. coli* DH5α harboring plasmid pLOT2	This study
ECOlot3	*E. coli* DH5α harboring plasmid pLOT3	This study
Pseudomonas aeruginosa		
PAO1	Wild type prototype	[126]
PAOsl2	PAO1 with unmarked Δ(*PA0102-orf*)	This study
PAOsl4	PAO1 with unmarked Δ(*PA0102 PA2053-orf*)	This study
PAOsl5	PAO1 with marked Δ(*PA0102 PA2053 PA4676-orf*)	This study
pEX100T	Ap^R; *oriT*$^+$ *sacB*$^+$ gene replacement vector	[54]
pPS856	Ap^R; Gm^R; 0.83-kb blunt-ended *Sac*I fragment from pUCGM ligated into the *Eco*RV site of pPS854	[52]
pFLP2	Ap^R; 2.6-kb *Bam*HI–*Sph*I fragment from pALB2 ligated between the same sites of pPS908	[52]
pLOT1	Δ(*PA0102-orf*) gene-deletion plasmid	This study
pLOT2	Δ(*PA0102 PA2053-orf*) gene-deletion plasmid	This study
pLOT3	Δ(*PA0102 PA2053 PA4676-orf*) gene-deletion plasmid	This study

atherosclerosis [13], however the mechanisms have not been characterized. Here we hypothesize that *Pseudomonas aeruginosa*, a human pathogen causing severe chronic infections, is capable of $CaCO_3$ deposition, which enhances the pathogenic impact of the organism.

Most commonly, soft tissue calcium deposits contain phosphates or carbonates. Deposition of calcium phosphate salts have been associated with metastatic calcification, hypervitaminosis D, tumoral calcinosis, arteriosclerosis, venous calcifications, and dermatomyositis [14,15]. $CaCO_3$ deposition has associated with collagen-vascular diseases [16], gallstones and kidney stones [17]. Several factors may lead to soft tissue $CaCO_3$ deposition. The key chemical factors include concentrations of Ca^{2+}, carbonate (CO_3^{2-}) and the availability of nucleation sites [18,19]. Biological factors include the metabolic activity providing CO_3^{2-} and increasing pH [20]. Several bacterial processes may generate CO_3^{2-}, including activity of CAs, nitrogen cycle, and urea hydrolysis [19,21,22]. Several studies have suggested that prokaryotes are able to form $CaCO_3$ precipitates in diverse natural environments such as soil, seawater, saline lakes and geological formations [23–26]. Most of these studies involve microbial communities, and only a few focus on pure cultures. The latter include a soil bacterium, *P. fluorescens* [27] and cyanobacterium *Synechocystis* sp. PCC 6803 [26]. The ability of *P. aeruginosa* to deposit calcium was observed during growth at 15 mM $CaCl_2$, however, the mechanisms of calcium salt deposition have not been studied. [28]

P. aeruginosa is an opportunistic pathogen that invades human tissues and cause life-threatening acute and chronic infections including pneumonia, bloodstream infections, urinary tract and surgical site infections. The best-studied cases are the infections of lung airways in CF patients, and burn wounds infections. *P. aeruginosa* is also one of the leading causes of infective endocarditis, particularly in intravenous drug users, young children, and patients with prosthetic valve replacement [29,30]. *P. aeruginosa* infections are considered biofilm-associated, where bacteria colonize tissue surface [31] and form biofilms, which have an increased resistance to antibiotics [32] and to host defenses [33,34]. Importantly, several diseases caused by *P. aeruginosa* chronic infections, including endocarditis, meningitis, and CF [35–39], are associated with calcification during their advanced stages of development.

The metalloenzymes, carbonic anhydrases (CAs), EC 4.2.1.1, catalyze the reversible hydration of CO_2 to HCO_3^- ($CO_2 + H_2O \rightleftharpoons HCO_3^- + H^+$). They are present in all domains of life and are involved in different physiological functions including pH homeostasis, CO_2/HCO_3^- transport, and carbon fixation (reviewed in [40]). Due to their catalytic activity, CAs may drive the formation of $CaCO_3$ under appropriate environmental conditions. The role of eukaryotic CAs in calcification has been shown in mollusks shells [41] and fish otoliths [42]. Membrane bound α-CA from coral *Stylophora pistillata* [43] and bovine CA [44] were shown to be involved in precipitation of $CaCO_3$. Several prokaryotic CAs including extracellular CA from *Bacillus sp* [45] and β-CA from *Citrobacter freundii* SW3 [46] were suggested to contribute to $CaCO_3$ formation, however these studies aimed biotechnological applications and lacked molecular understanding. Previously, we showed that *P. aeruginosa* PAO1 encodes three functional β-CAs designated psCA1, psCA2, and psCA3 [47]. Metal and enzymatic analyses of the His-tag purified β-CAs confirmed that the proteins contain zinc, required for catalytic activity, and catalyze the hydration of CO_2 to bicarbonate [47]. We also characterized the crystal structure of psCA3 and identified several inhibitors binding the catalytic site that inhibit the activity of the enzyme [48,49].

In this study, we identified the mechanism of calcium deposition in a human pathogen, *P. aeruginosa,* by applying transmission electron microscopy (TEM) with X-ray elemental analysis and gene deletion followed by fluorescent microscopy. We also performed inhibition studies and *in -silico* modeling to characterize the role of the three β-CAs expressed by *P. aeruginosa* PAO1 in the formation of calcium deposits and virulence.

2. Materials and methods

2.1. Bacterial strains, plasmids, and media

The bacterial strains and plasmids used in this study are listed in Table 1. All the cultures were stored in 10% (v/v) skimmed milk at −80 °C. PAO1 was grown at 37 °C in biofilm minimal medium (BMM) [50], which contained (per liter): 9.0 mM sodium glutamate, 50 mM glycerol, 0.02 mM $MgSO_4$, 0.15 mM NaH_2PO_4, 0.34 mM K_2HPO_4, and 145 mM NaCl, 20 µl trace metals, 1 ml vitamin solution. Trace metal solution (per liter of 0.83 M HCl): 5.0 g $CuSO_4.5H_2O$, 5.0 g $ZnSO_4.7H_2O$, 5.0 g $FeSO_4.7H_2O$, 2.0 g $MnCl_2.4H_2O$. Vitamins solution (per liter): 0.5 g thiamine, 1 mg biotin (Goldbio). The pH of the medium was adjusted to 7.0. When needed, 5 mM $CaCl_2.2H_2O$ (Sigma) was added. All reagent-grade chemicals were purchased from ThermoFisher Scientific (Waltham, MA) or Sigma-Aldrich (St. Louis, MO), unless otherwise indicated.

For DNA manipulations, *E. coli* and *P. aeruginosa* cultures were grown in Luria–Bertani (LB) broth (per liter: 10 g tryptone, 5 g yeast extract, 5 g NaCl) at 37 °C with shaking at 200 rpm. Antibiotics used for *E. coli* were (per ml) 100 µg ampicillin (Ap) or 30 µg gentamycin (Gm); for *P. aeruginosa*, (per ml) 300 µg carbenicillin (Cb), 60 µg tetracycline (Tet) or 100 µg Gm.

2.2. Standard DNA procedures

Established DNA manipulation procedures were performed as described in [51]. Plasmid DNA was isolated using the QIAprep Mini-spin kit, and chromosomal DNA was obtained using the Wizard® Genomic DNA Purification Kit (Promega). DNA fragments were purified from agarose gels using the QIAquick gel extraction kit. DNA concentration was determined spectrophotometrically using NanoDrop 1000 Spectrophotometer (Thermo Scientific, Waltham, MA). DNA transformation into *E. coli* DH5α and *P. aeruginosa* PAO1 was performed using heat shock or electroporation protocols [51,52].

2.3. Generation of unmarked single, double, and triple gene deletions

Gene deletions were generated following the procedures in [52–54] with modifications. To generate constructs for gene replacement, the upstream (UP) and downstream (DN) gene flanking fragments as well as gentamycin resistance cassette (GmΩ) were PCR amplified. The UP and DN regions immediately flanking *psCA1, psCA2,* or *psCA3* were amplified using 50 ng chromosomal PAO1 DNA in a 50 µl PCR reaction mix containing 5x Phusion® HFbuffer, 200 µM dNTPs, 0.5 µM of each primer (Table 2, Fig. 1A.), 3% DMSO and 0.4 units of Phusion® High-Fidelity DNA polymerase (New England Biolabs). The 5′ ends of the primers contained 21 bases of the plasmid pEX100 T (UP forward), 25 bases of the GmΩ (UP reverse), 24 bases of the GmΩ (DN forward), or 23 bases of pEX100 T (DN reverse) (Table 2, Fig. 1A). The 3′ ends of the primers contained 20–24 bases from the UP or DN regions of the corresponding target genes. The PCR conditions were 98 °C for 30 s, followed by 30 cycles of 98 °C for 10 s, 60 °C for 30 s, and 72 °C for 30 s and a final extension at 72 °C for 10 min. To amplify the GmΩ with flanking *FRT* sites, a similar PCR reaction was set using purified pPS856 as a template DNA [52] and Gm-F and Gm-R primers (Table 2, Fig. 1B.). The PCR conditions were 98 °C for 30 s, followed by 30 cycles of 98 °C for 10 s, 60 °C for 30 s, and 72 °C for 45 s, and a final extension at 72 °C for 10 min. The resulting PCR products were verified by gel electrophoresis and, when needed, purified using QIAquick gel extraction kit.

Table 2
PCR primers used in this study.

Name	Sequence (5' → 3')
psCA1-UpF-pEX100T*	TCATTACCCTGTTATCCCTACtagctggctggcaccgggcggc
psCA1-UpR-Gm	TCAGAGCGCTTTTGAAGCTAATTCGcatggttcggaacctcgatgag
psCA1-DnF-Gm	AGGAACTTCAAGATCCCCAATTCGtagcggcggccgtgcgggccg
psCA1-DnR-pEX100T*	TAGGGATAACAGGGTAATCCCGGcggcagggcgacgaggaacac
psCA2-UpF-pEX100T*	TCATTACCCTGTTATCCCTACtcgccggcatcggtgggacgc
psCA2-UpR-Gm	TCAGAGCGCTTTTGAAGCTAATTCGcatggcgctgggctcctggccg
psCA2-DnF-Gm	AGGAACTTCAAGATCCCCAATTCGatcccttccctcacaaccac
psCA2-DnR-pEX100T*	TAGGGATAACAGGGTAATCCCGGgccgccgggaatgctgccgc
psCA3-UpF-pEX100T*	TCATTACCCTGTTATCCCTACgagtccccctggtggcgcttcg
psCA3-UpR-Gm	TCAGAGCGCTTTTGAAGCTAATTCGcatggcatgcccctcgtttgac
psCA3-DnF-Gm	AGGAACTTCAAGATCCCCAATTCGgagaggcggaagctctttc
psCA3-DnR-pEX100T*	TAGGGATAACAGGGTAATCCCGGgacgagccgggcaacaagatcg
Gm-F§	CGAATTAGCTTCAAAAGCGCTCTGA
Gm-R§	CGAATTGGGGATCTTGAAGTTCCT
pEX100T-sacB-F	TCGCGCGTTTCGGTGATG
pEX100T-sacB-R	GCAGGCAAGACCTAAAATGTG
psCA1-F	AGAGAGCATATGCCAGACCGTATG
psCA1-R	AGAGAGGGATCCTCACGAGCTCAG
psCA2-F	AGAGAGCATATGCGTGACATCATCG
psCA2-R	AGAGAGGGATCCTCAGGCGAC
psCA3-F	AGAGAGCATATGAGCGACTTGCAG
psCA3-R	AGAGAGGGATCCTCAGCAGCAAC
pEXUPseq-F	CGATTAAGTTGGGTAACGCCAG
pEXUPseq-R	GCACATCAGCTTCAAAAGCGCTC
pEXDNseq-F	CGAGCTATCCATTGCTGTTG
pEXDNseq-R	GTTAGCTCACTCATTAGGCAC

Sequences in capital letters are common for all genes amplified and overlap with the GmΩ or pEX100Tprimer sequences. Lower-case letters indicate UP or DN target gene-specific sequence. *The overlap pEX100 T region in the primers includes the recognition site for *XmaI* (underlined). §The Gm primer sequence is obtained from [53].

To assemble the obtained DNA fragments into a construct, Gibson cloning was used [55]. We used 5X buffer containing 25% PEG-8000, 500 mM Tris-HCl pH 7.5, 50 mM $MgCl_2$, 50 mM DTT, 1 mM dATP, 1 mM dTTP, 1 mM dCTP, 1 mM dGTP, 5 mM NAD and nuclease free water to make up to a total volume of 2 ml. A 1.33X Gibson Cloning Master mix was made by mixing 100 µl of 5X isothermal reaction buffer, 2 µl of 1 U/µl T5 exonuclease, 6.25 µl of 2 U/µl Phusion DNA polymerase, 50 µl of 40 U/µl Taq DNA ligase and 216.75 µl of nuclease free water to make a final volume of 375 µl. Master mix was stored in 15 µl aliquots at -20 °C. For Gibson assembly, 5 ul of equimolar amounts of the three gene specific DNA fragments (UP DN, and GmΩ, Fig.1C) were mixed with 15 µl of 1.33 X master mix and incubated for 1 h at 50 °C. The assembled constructs LOT1 (1,793 bp), LOT2 (1,746 bp), and LOT3 (1,750 bp) for *psCA1, psCA2,* and *psCA3*, correspondingly, were purified by using QIAquick gel extraction kit and set for the second Gibson assembly with the addition of 50 ng of *XmaI* digested pEX100 T vector. Alternatively, the products were PCR amplified and ligated into 50 ng of *SmaI* digested pEX100 T using the Blunt/TA ligase master mix. The resulting vectors were designated pLOT1, pLOT2, and pLOT3 (Table 1, Fig. 1D) and transformed into *E. coli* DH5α. The successful transformants were selected on Gm containing LB agar plates and verified by colony PCR using pEXUPseq_F/ pEXUPseq_R and pEXDNseq_F/pEXDNseq_R primers (Table 2) and sequenced. The confirmed clones designated as EcoLot1, EcoLot2, and EcoLot3.

To delete the first gene, *psCA1*, the gene-knockout plasmid pLOT1 was transformed into *P. aeruginosa* PAO1 by electroporation. Successful transformants were selected on LB-Gm agar plate. A SacB-based counter-selection was used to select the double crossover events during growth in 5–8 % sucrose resulting in Gm^R $Sucrose^R$ phenotype. The selected Gm^R $Sucrose^R$ Cb^S colonies were considered as putative deletion mutants, which were confirmed by colony PCR using three sets of primers: Gm-F/Gm-R, pEX100TsacB-F/pEX100TsacB-R, and *psCA1*-F/*psCA1*-R (Table 2, Fig. 1). The confirmed mutant strain lacking *psCA1* was named PAOsl1 (Table 1). To remove the GmΩ cassette from PAOsl1 and generate an unmarked deletion, PAOsl1 was transformed with pFLP2 encoding Flp recombinase [52]. The transformants were selected on LB-Cb agar plate and subjected to SacB counter-selection for curing from the plasmid. The clones with $Sucrose^R$ Gm^S Cb^S phenotypes were selected and PCR verified using Gm-F/Gm-R primers (Table 2) to confirm the loss of the GmΩ cassette. The final markerless *psCA1* lacking mutant was designated PAOsl2. The double mutant lacking *psCA1 and psCA2* designated as PAOsl4 and the triple mutant lacking all three *psCAs* designated as PAOsl5, were generated following similar procedures using PAOsl2 and PAOsl4 as the background strains, correspondingly. For convenience, here we named the single, double, and triple mutants as SM, DM, and TM, correspondingly.

2.4. Quantification of calcium deposition

To measure the quantities of Ca^{2+} ions from calcium salt deposits, three approaches were applied: scraping deposits followed by solubilization and Ca^{2+} quantification, measuring reduction of free Ca^{2+} in the medium, and microscopy. For the first approach, cultures were grown in glass tubes with 5 ml BMM medium with no added or 5–10 mM $CaCl_2$ for 24–48 h. The optical densities (OD_{600}) of the cultures were measured, and the cells were pelleted for total protein yield measurements. The glass tubes were rinsed three times with nano-pure water to remove cells and air-dried at room temperature (RT). The material deposited on the walls of the tubes was solubilized with 250 µl of 0.5 M HCl. To

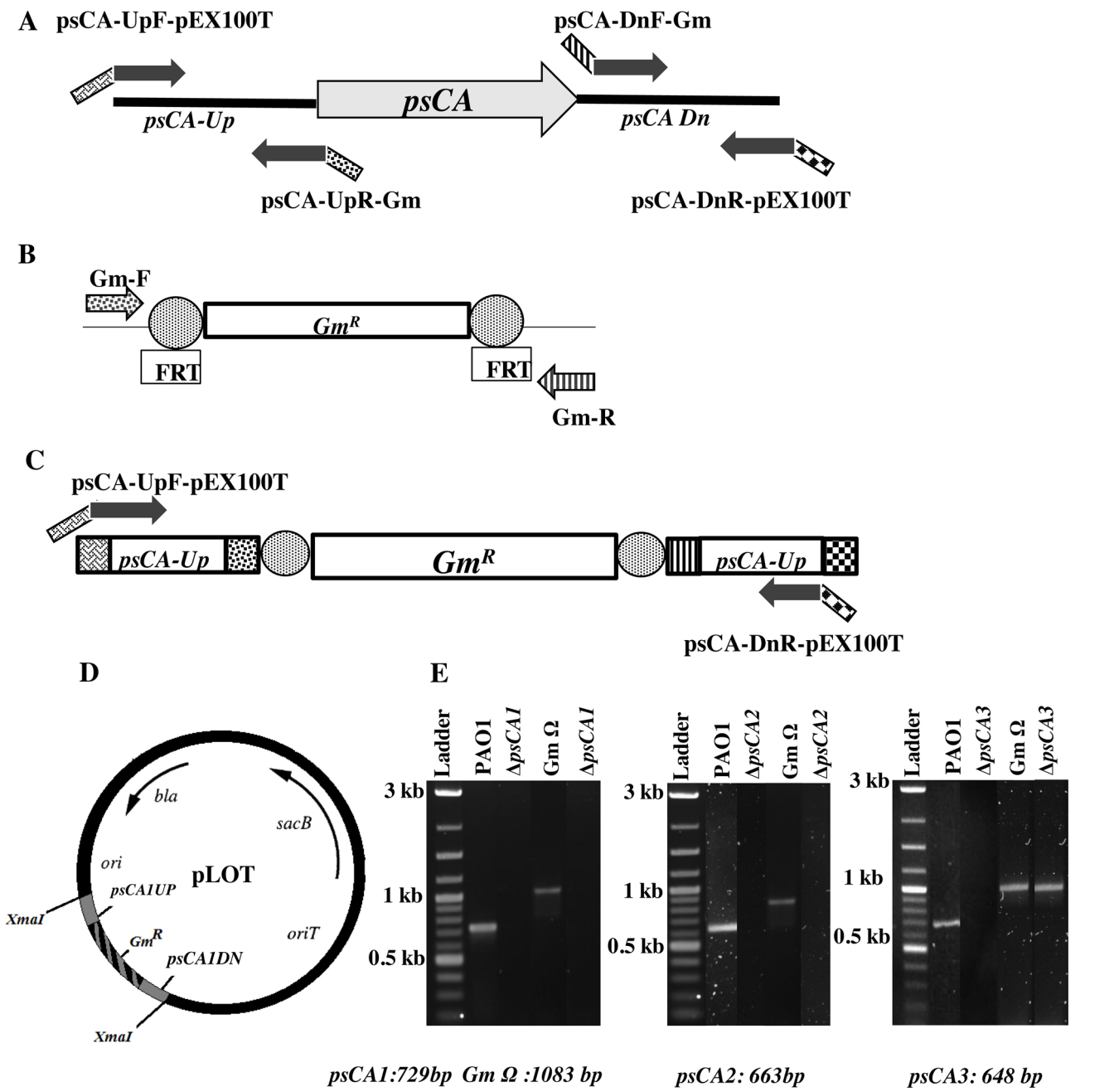

Fig. 1. Gene deletion strategy and verification of the mutants. A. Primer design for amplifying upstream and downstream regions of each of three carbonic anhydrase (CA) genes (*psCA1, psCA2,* and *psCA3*). Primers bear portions specific for the cloning vector pEX100 T as well as for the gentamicin resistance cassette (Gm^R). B. Primers design for amplifying Gm^R. C. The UP-Gm^R- DN construct for replacing each CA with Gm^R. D. The UP-Gm^R- DN construct cloned into XmaI restriction site of pEX100 T. E. PCR verification of deletion of *psCA1, psCA2* and *psCA3.*

maximize the recovery, the mixtures were vortexed for 2 min and water-bath-sonicated for 5 min. The amount of free Ca^{2+} was quantified using QuantiChrom™ calcium assay kit (Bioassay) following the manufacture's protocol. To measure total protein yield, the pelleted cells were lysed by boiling at 90 °C for 10 min in 100 µl of 1 N NaOH and subjected to Modified Lowry Protein assay (Pierce) with bovine serum albumin as a protein standard. The measured Ca^{2+} concentrations were normalized by total cell protein (mM Ca^{2+}/mg of protein). Non-inoculated negative controls underwent the same treatment and showed no calcium salt deposition. The data represent the mean values of at least three biological replicates.

2.5. Measurement of free Ca^{2+} ions

To measure changes in free Ca^{2+}, cultures were grown in glass tubes at 37^0C with 5% CO_2 with or without shaking in 5 ml BMM medium supplemented with 5 mM or 10 mM $CaCl_2$. The optical densities (OD_{600}) of the cultures were measured, and the cells were pelleted for total protein yield measurements. One ml of supernatant was saved in -20^0C for subsequent estimation of free Ca^{2+} by using QuantiChrom™ calcium assay kit following the manufacture's protocol. The changes in free Ca^{2+} were calculated as % of remaining Ca^{2+} (considering the initially added Ca^{2+} from $CaCl_2$ as 100%).

2.6. Transmission electron microscopy (TEM) and X-ray elemental analysis

Cultures were grown in 50 ml BMM medium with no added or 10 mM calcium for 12 h, pelleted at 2800 × *g* for 5 min at 4 °C, and cell pellets were discarded. The supernatants were spun at 116,666-x *g* for 15 min at RT using the Beckman® L8-70 M ultracentrifuge (Beckman Coulter, Inc., Indianapolis, IN), and the pellets were collected and mixed with 20 µl of the supernatants. Approximately 5 µl of the samples was loaded on 150 mesh C-CO grid (Electron Microscopy Sciences, Hatfield, PA) and allowed to air dry at RT for 15–20 min. The remaining liquid was removed gently by touching the grid at the bottom with a filter paper. The subjected samples were observed using the JEOL JEM-2100 200 KV Electron Transmission Microscope with Evex EDS (Evex Analytical Instruments Inc., Princeton, NJ) at the Oklahoma State University Microscopy Facility (Stillwater, OK) at a magnification of 8,000x-25,000x, and HV of 200KV. The detected deposits were then subjected to Evex energy-dispersive X-ray (EDX) microanalysis with fully quantitative analysis software package that includes X-ray mapping capabilities; Evex liquid-nitrogen-free Quantum Dot Detector with energy resolution of 128 FWHM (Evex Analytical Instruments Inc., Princeton, NJ) to study their composition.

2.7. Fluorescence microscopy for detecting Ca^{2+} ion deposition

For fluorescence microscopy, bacterial biofilms were grown on sterilized coverslips placed in 6-well plates, each containing 7 ml BMM supplemented (or not) with 10 mM $CaCl_2$ for 48 h at 5% CO_2 without shaking. At the end of incubation, the medium was removed, and the coverslips in the wells were washed twice gently with 1 ml of saline. Each coverslip was then stained with 60 µl of stain mixture composed of 50 µl saline, 4 µl DAPI (4′,6-diamidino-2-phenylindole) (Invitrogen) and 6 µl Fluo-4 (1 mM stock in water) (Invitrogen) for an 1 h in dark. DAPI was used to stain cellular DNA, and Fluo-4 to stain Ca^{2+} [56]. Following staining, each coverslip was washed twice with saline, mounted on top of a glass slide and examined using the Nikon NI-E epifluorescent microscope equipped with a 100 × 1.45 NA objective, Zyla 4.2plus camera and DAPI, DIC, and GFP filers operating NIS Elements software. The images were analyzed by using ImageJ version 2.0. Samples were protected from light at all time to prevent photodegradation.

2.8. Gene expression analysis by RT-qPCR

To characterize the transcriptional profiles of *psCA1* gene, RT-qPCR was performed. Total RNA was isolated from *P. aeruginosa* PAO1 grown in BMM with no added or 5 mM calcium using RNeasy Protect Bacteria Mini kit (Qiagen) following the manufacturer's protocol. PAO1 was grown until middle-log phase (13 h; OD_{600} 0.2), and 15 ml of the culture was used for RNA isolation. DNase treatment was performed using column-based kit (Qiagen) and Turbo DNase treatment (Ambion). The absence of genomic DNA (gDNA) was confirmed by conventional PCR and real time quantitative PCR (RT-qPCR) using *16SrRNA* primers. RNA yield was measured using NanoDrop spectrophotometer (NanoDrop Technologies Inc.), and the quality of the purified RNA was assessed by Bioanalyzer 2100 (Agilent) and 1% agarose gel electrophoresis. Following the MIQE guidelines [57], only the RNA samples with an OD_{260}/OD_{280} ratio of 1.8–2.0 and an RIN value of ≥ 9.0 was taken for further analyses. A total amount of 6 µg – 20 µg of RNA was purified from each sample. RNA samples were stored at −80 °C.

Primers for *psCA1* (PA0102) were designed using Primer3 Plus [58] and Primer BLAST [59]. Primers were tested *in-silico* for secondary structure formation using IDT oligoanalyzer. Their specificity was tested by BLAST alignments against *Pseudomonas* genome available at www.pseudomonas.com and confirmed by conventional PCR and RT-qPCR melt curve analysis. Primer efficiency was calculated using linear regression curve analysis. For this, RT-qPCR was performed for each primer pair using 10-fold serial dilution of gDNA, and the obtained Cp values were plotted. Primers with an R^2 value of 0.99 and an efficiency of 93 (efficiency of the primer for the control gene) ± 10% were accepted for further work according to the MIQE guidelines [57]. The efficiency of the selected primers was 97%. Four housekeeping genes, *rpoD*, *rpoS*, *proC* and *16SrRNA* [60,61] were selected and tested for their transcriptional response to added Ca^{2+}. The transcription of *16SrRNA* gene was not affected by addition of Ca^{2+} and therefore this gene was selected as a control. Due to the low Cp value of *16SrRNA* (≤ 8 for 5 ng of cDNA), transcriptional profiling for this gene was done using 10 fold diluted cDNA. Reverse transcription of total RNA (1 µg) was performed using Transcriptor First Strand cDNA Synthesis Kit (Roche) according to the manufacturer's protocol and stored at -20 °C. RT-qPCR was run using 5 µl of SYBR green master mix (Roche, Indianapolis, IN), 0.5 µM of each primer and 5 ng of nucleotides added to a total volume of 10 µl of reaction mixture in 384 well plates sealed with Light Cycler 480 Sealing Foil (Roche, Indianapolis, IN) in Roche Light Cycler 480. At least five technical replicates for each biological replicate and a minimum of three biological replicates for every sample were analyzed. A no-template control was used as negative control. The cycle included 10 min denaturation at 95 °C followed by 35 cycles of 95 °C for 10 s, 61 °C for 15 s, and 72 °C for 10 s. A fold change in gene transcription was calculated using $2^{-\Delta\Delta Ct}$ method [62]. Statistical analysis was performed by using two-tailed *t*-test assuming equal variances.

2.9. Immunoblot analysis

P. aeruginosa PAO1 cells were grown to mid-log and harvested. Cell pellets were washed twice with saline, resuspended in 20 mM Tris buffer (pH 8.3), containing 1:100 [vol/vol] complete Mini protease inhibitor cocktail, and disrupted using FastPrep® bead beater (MP Biomedicals, Solon, OH) in five 15-sec cycles at a maximum speed, with 5 min on ice between the cycles. Cell extracts (5 µg) were separated by 12% SDS/PAGE gels and electroblotted onto polyvinylidene difluoride (PVDF) membranes (Immobilon; Millipore, Billerica, MA) using Biorad Trans-Blot® SD Electrophoretic Transfer Cell unit following manufacturer's protocols. The membranes were probed with primary antiserum raised to β-class Cab from *M. thermoautotrophicum* ΔH (43) (generously shared by Dr. James Ferry, Pennsylvania State University). Goat anti-mouse immunoglobulin G, conjugated to Alexa Fluor® 680 (Molecular Probes, Eugene, OR), was used as the secondary antibody. Antibody binding was detected by Odyssey infrared imager (LI-COR, Lincoln, NE). Coomassie-stained gels were run in parallel as loading controls. As controls, we used recombinantly expressed and His-tag purified psCA1, psCA2, and psCA3 proteins. Proteins were purified as earlier described in [63].

2.10. CA enzyme inhibition assay

The catalytic activities of the His-tag purified psCA1, psCA2, and psCA3 were measured by monitoring CO_2 hydration reaction using Sx.18Mv-R Applied Photophysics (Oxford, UK) stopped-flow instrument [64]. Phenol red (at a concentration of 0.2 mM) was used as indicator, working at the absorbance maximum of 557 nm, with 10 mM TRIS (pH 8.3), 0.1 M Na_2SO_4 (for maintaining constant ionic strength). The CA-catalyzed CO_2 hydration reaction was monitored for a period of 10 s at 25 °C. The CO_2 concentrations ranged from 1.7 to 17 mM for the determination of the kinetic parameters and inhibition constants. For each inhibitor at least six traces of the initial 5–10% of the reaction have been used for determining the initial velocity. The uncatalyzed rates were determined in the same manner and subtracted from the total observed rates. Stock solutions of inhibitors (10 mM) were prepared in distilled-deionized water and dilutions up to 1 nM were done thereafter with the assay buffer. Enzyme and inhibitor solutions were pre-incubated together for 15 min (standard assay at room temperature) prior to assay, in order to allow for the formation of the enzyme–inhibitor complex. The inhibition constants were obtained by non-linear least-

squares methods, using GraphPad PRISM 3 and the Cheng–Prusoff equation, as reported earlier [65–68]. All CAs were recombinant proteins produced as reported earlier by our groups [69–71].

2.11. In-silico model analysis

A structural characterization of the three β-class CAs: psCA1, psCA2, and psCA3 was done to compare the CAs active sites. The models were built using the online server SWISS-MODEL (https://swissmodel.expasy.org/). The X-ray crystal structure of psCA3 (protein database (PDB ID: 4RXY) [48,49] was used as the template to generate the *in-silico* model structures of psCA1 and 2. The calculated models superimposed on the psCA3 template crystal structure using the molecular graphics programs Coot [72] and PyMOL (PyMOL Molecular Graphics System, Version 1.5.0.4 Schrödinger, LLC) to observe differences in active site amino acids and predict the potential impact on enzyme activity.

2.12. Virulence assay

To evaluate the impact of Ca^{2+} ions and *psCA1* on *P. aeruginosa* virulence, *Galleria melonella* infection model was used as described in [73] with modifications. *P. aeruginosa* PAO1, and *ΔpsCA1* mutant were grown for 12 h in BMM with 10 mM or no added calcium. For inhibition studies, AAZ at the concentration of 100μM was added. The cultures were normalized to an OD_{600} of 0.1, from which a series of 10^{-1} to 10^{-6} dilutions was generated in phosphate buffered saline (PBS) with the corresponding $CaCl_2$ or AAZ concentrations. To verify the infectious dose, 10 μl from the dilutions 10^{-4}, 10^{-5} and 10^{-6} were spread on LB plates, grown overnight at 37 °C, and the colony forming units (CFU) were counted. Active *G. mellonella* larvae (Speedy Worms or American Cricket Ranch) stored in the dark at 4 °C and starved for no more than 48 h were gently washed with 70% ethanol and 1 mg/mL rifampicin. Ten experimental worms were injected with 5 μL of cell suspension grown at no added or 10 mM $CaCl_2$ with or without 100μM AAZ and normalized to contain 2 or 10 CFU. Five more were injected with 5 μL of PBS at the corresponding $CaCl_2$ or AAZ concentrations as non-infected controls. The worms were incubated at 37 °C for 24 h and monitored for death every 2 h. Times of death (TOD) were recorded for each worm. Dead worms were placed in 1.5 ml microcentrifuge tubes and frozen at -20 °C for further analyses. Additionally, five worms were injected for each condition and collected after 10 h of incubation for the assessment of Ca^{2+} concentration in the collected hemolymph. The collected hemolymph samples (~15 μL) were centrifuged at 1500 *g* for 10 min at 4 °C and diluted tenfold in Tris-buffered saline (50 mM Tris-HCl pH 6.8, 1 mM NaCl). To estimate the levels of free Ca^{2+} in the hemolymph samples, 5 μL of the hemolymph samples were subjected to QuantiChrom™ calcium assay kit following the manufacturer's protocol.

3. Results

3.1. P. aeruginosa PAO1 deposits calcium salts

To study the ability of *P. aeruginosa* PAO1 to deposit calcium, we applied four independent approaches: measuring reduction of free Ca^{2+} in the medium, scraping deposits from the surface of glass tubes followed by Ca^{2+} quantification, Fluo-4 staining followed by fluorescence microscopy, and electron microscopy followed by X-ray microanalysis. First, to confirm that PAO1 is able to deposit calcium, we collected the supernatants of cells grown in the presence of 10 mM $CaCl_2$, and subjected to Transmission Electron Microscopy (TEM) followed by X-ray elemental analysis. TEM detected the presence of deposits in oval shape, and about 0.1-0.2 μm in size (Fig. 2A). No deposits were detected in the cultures grown at no added $CaCl_2$ or non-inoculated controls, proving that PAO1 cells are responsible for calcium deposition. The following X-ray elemental analysis confirmed that the deposits contained calcium (Fig. 2B).

We also tested calcium deposition by *P. aeruginosa* biofilms, which were grown on glass coverslips and stained with DAPI. Calcium depositions were detected by staining with Fluo-4, which fluoresces green upon Ca^{2+}-binding [56]. We observed that only in the presence of 10 mM $CaCl_2$, cells were stained with both blue DAPI and green Fluo-4 (Fig. 3A), confirming deposition of calcium. We did not observe Fluo-4 stained calcium deposition outside of cells, likely due to their small size. Instead, entire cells were stained with Fluo-4, suggesting that calcium salts were deposited on cell surfaces. Unstained controls for background fluorescence and stained no-cells controls showed no significant contribution to the Fluo-4 signal intensity.

3.2. Static growth at 5% CO_2 favors calcium deposition

In order to determine the conditions that favor calcium deposition, PAO1 cells were grown in flasks in BMM with the addition of 5 mM, 10 mM, or no added $CaCl_2$ for 36–48 h. Considering that deposits may be disrupted by shaking at 200 rpm, commonly used for aeration, and the prediction that carbonic anhydrases are involved in the deposition, growth at no shaking (static) in the presence of 5% CO_2 was tested and compared to growth at shaking in ambient air. The changes in free Ca^{2+} in the medium were measured (Fig. 4). We observed a temporal gradual decrease in free Ca^{2+} during growth under static conditions measured (Fig. 4A). After 36 h of incubation, only 20–27 % of Ca^{2+} remained in the medium, which initially contained 5–10 mM Ca^{2+}. No changes in free Ca^{2+} were observed in shaking cultures (Fig. 4B). These data support the notion that static incubation in the presence of 5% CO_2 favors deposition of calcium salt by PAO1. Therefore all the following experiments were performed under these conditions.

3.3. P. aeruginosa β-CA psCA1 plays role in calcium deposition

Previously we reported that *P. aeruginosa* PAO1 produces three enzymatically active β-CAs designated as psCA1, psCA2, and psCA3 [47]. To test whether psCAs are involved in calcium deposition, we generated deletion mutants lacking *psCA1* alone, both *psCA1* and *psCA2*, or all three *psCAs* (Fig. 1).

To test whether the deletion of β-CAs has any effect on PAO1 fitness during growth, we monitored growth of the mutants at different Ca^{2+} levels under two conditions: i) static at 5% CO_2 and ii) shaking at ambient CO_2. There was no difference in growth during static incubation in 5% CO_2. However, under shaking conditions in ambient CO_2, growth of the double and triple mutants was delayed by 3 and 4 h, respectively. Similar delays were observed when 5 or 10 mM $CaCl_2$ was added to the medium. (Supplementary Fig. S1).

To examine the role of β-CAs in calcium deposition, the mutants lacking individual or multiple *psCAs* were tested and compared to the wild type, PAO1. For this, the cultures were grown in glass tubes at 5 mM or 10 mM $CaCl_2$ for 48 h without shaking in the presence of 5% CO_2. Calcium deposition was measured by both collecting culture supernatants and scraping deposited calcium salt, followed by QuantiChrom Ca^{2+} assay as described in the Methods. In agreement with the TEM (Fig. 2) and the measurements of Ca^{2+} in the supernatants in flask cultures (Fig. 4), the levels of Ca^{2+} in the supernatants of PAO1 grown in tubes reduced by 56% and 66% when the initial BMM contained 5 or 10 mM $CaCl_2$, respectively (Fig. 5A). This reduction in free Ca^{2+} correlated with the deposition of calcium on the test tube walls, which reached 0.35, and 0.75 mM Ca^{2+}/mg of cellular protein at 5 and 10 mM $CaCl_2$ added to the initial growth medium, respectively (Fig. 5B). The deletion of *psCA1* significantly decreased calcium deposition. There was only 15% and 3% decrease in the free Ca^{2+} levels for the mutant at 5 and 10 mM $CaCl_2$, correspondingly (Fig. 5A). Furthermore, the mutant showed a 34 and 46% decrease in the amounts of deposited calcium (Fig. 5B). Additional deletion of *psCA2* and *psCA*3 did not further impact the ability of the organism to

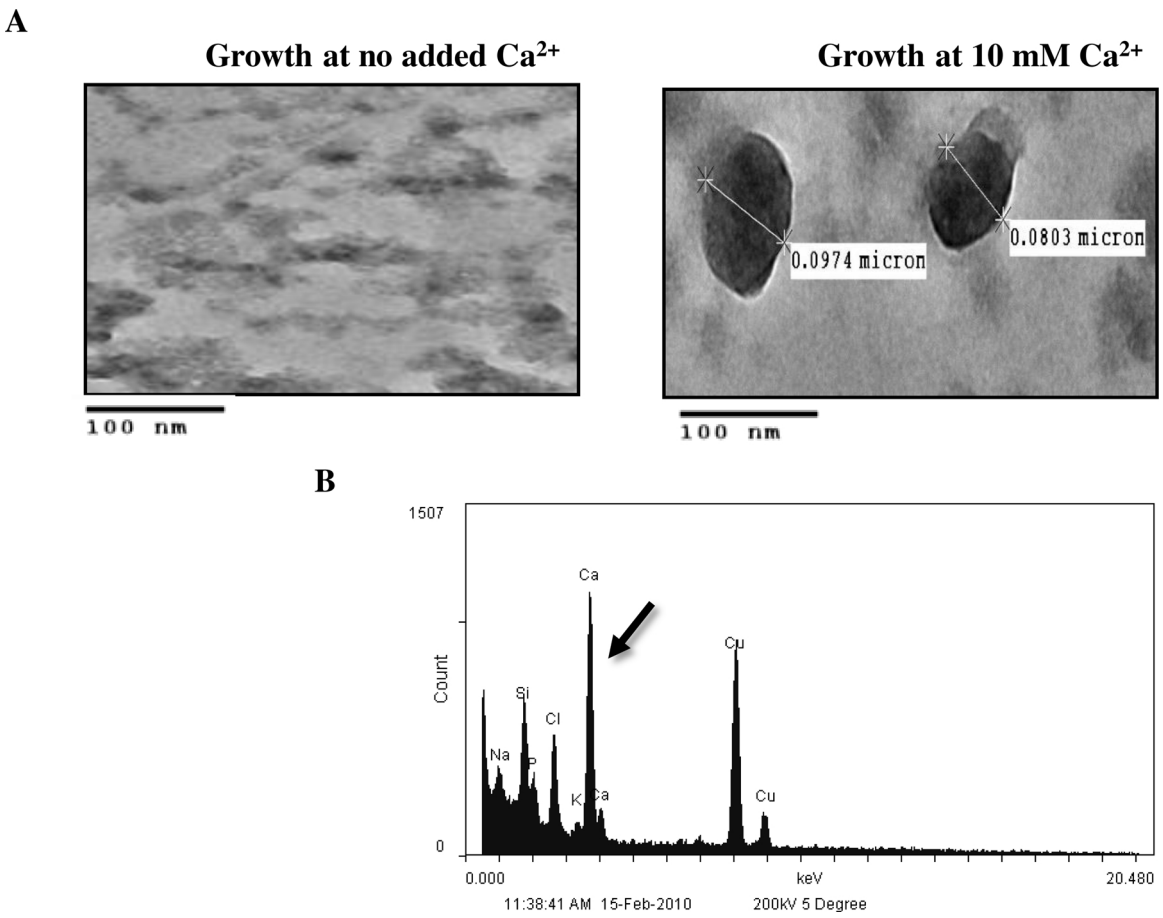

Fig. 2. Deposition of calcium by *P. aeruginosa* PAO1. A. Transmission Electron microscopy (TEM) images showing calcium deposits formed by PAO1 after growth in BMM supplemented with $CaCl_2$. B. X-ray elemental analysis confirming the presence of calcium (shown with an arrow) in the deposits formed by PAO1.

deposit calcium. This suggested that psCA1 is the main contributor and is required for calcium deposition in PAO1.

We validated the role of psCA1 in calcium salt deposition by fluorescence microscopy, comparing Fluo-4 stained calcium deposition by the Δ*psCA1* and PAO1 wild type grown as biofilms on the surface of glass coverslips (Fig. 3B). In contrast to PAO1 cells showing bright green fluorescence, the mutant cells were not fluorescent after staining with Fluo-4 when grown in the presence of 10 mM $CaCl_2$.

3.4. Kinetic and inhibition studies

Carbonic anhydrase activity for recombinant purified psCA1 was measured and compared to that of several eukaryotic CAs. At pH 8.3, a k_{cat} of 1.8×10^5 and a k_{cat}/K_m of 7.5×10^7 M^{-1} s^{-1} indicated that the enzyme is moderately active and based on the activity can be grouped with β-class Can2 from *Cryptococcus neoformans* and α-class human cytosolic isozyme hCA1 (Table 3).

A set of inorganic anions and small molecules known to interact with CAs, as well as sulfonamides and clinically used drugs, were assayed as potential inhibitors of psCA1 (Tables 4 and 5). The inhibition data showed that halides, as well as sulfates, perchlorate, tetrafluoroborate, fluorosulfonate did not inhibit psCA1 up to concentrations above 100 mM. Weak inhibition (K_I in the range of 1–12.5 mM) was observed for ions, including azide, bicarbonate, carbonate, nitrate, bisulfite, and diphosphate (Table 4). Bicarbonate inhibited about threefold weaker than carbonate. Other anions, such as cyanate, cyanide, nitrite, and sulfide were more effective, with K_I ranging from 0.5 to 1.0 mM. Four compounds, including sulfamide (SA), sulfonic acid, phenylboronic acid, and benzenearsonic acid showed much stronger inhibition with K_I within 9–80 μM range. Among them, SA is particularly promising with K_I of 9 μM, which is 126 fold stronger than that for a human isozyme hCA II (Table 4). Sulfonamides and clinically used drugs were overall further more effective in inhibiting psCA1 activity with K_I ranging at nano- to micro-molar levels. However, the most potent psCA1 inhibitor was 3-amino-benzene sulfonamide (compound 1, ABS) with K_I of 19 nM followed by ethoxzolamide (EZA), acetazolamide (AAZ), dorzolamide (DZA), and benzene-1, 3-disulfonamide (compound 3) with K_I in the range of 32–39 nM (Table 5). Compound 1 (ABS) is of particular interest as it inhibits psCA1 16-fold stronger than the tested human isozyme hCA II.

3.5. Inhibiting psCA1 reduces calcium salt deposition by PAO1

Considering that ABS, AAZ, and SA strongly inhibit psCA1, which is required for calcium deposition, we hypothesized that addition of these inhibitors during PAO1 growth would reduce calcium deposition. We have tested this hypothesis by measuring free Ca^{2+} and deposited calcium during PAO1 growth in the presence of these inhibitors (Fig. 6). AAZ showed the largest impact on calcium salt deposition. Only about 5% of free Ca^{2+} was removed from the medium (Fig. 6A), and the amount of Ca^{2+} deposited as a salt reached only 21% of that deposited by PAO1 grown without inhibitors (Fig. 6B). The addition of SA and ABS also reduced calcium deposition by 42 and 24%, which was reflected in 12 and 20% of free Ca^{2+} removal, respectively. We also tested the effect of inhibitors on calcium deposition in PAO1 biofilms. Upon staining with Fluo-4, non-treated PAO1 cells exhibited bright green fluorescence at 10 mM $CaCl_2$. However, in the presence of 100μM of AAZ, ABS or SA, we observed no green fluorescence above the

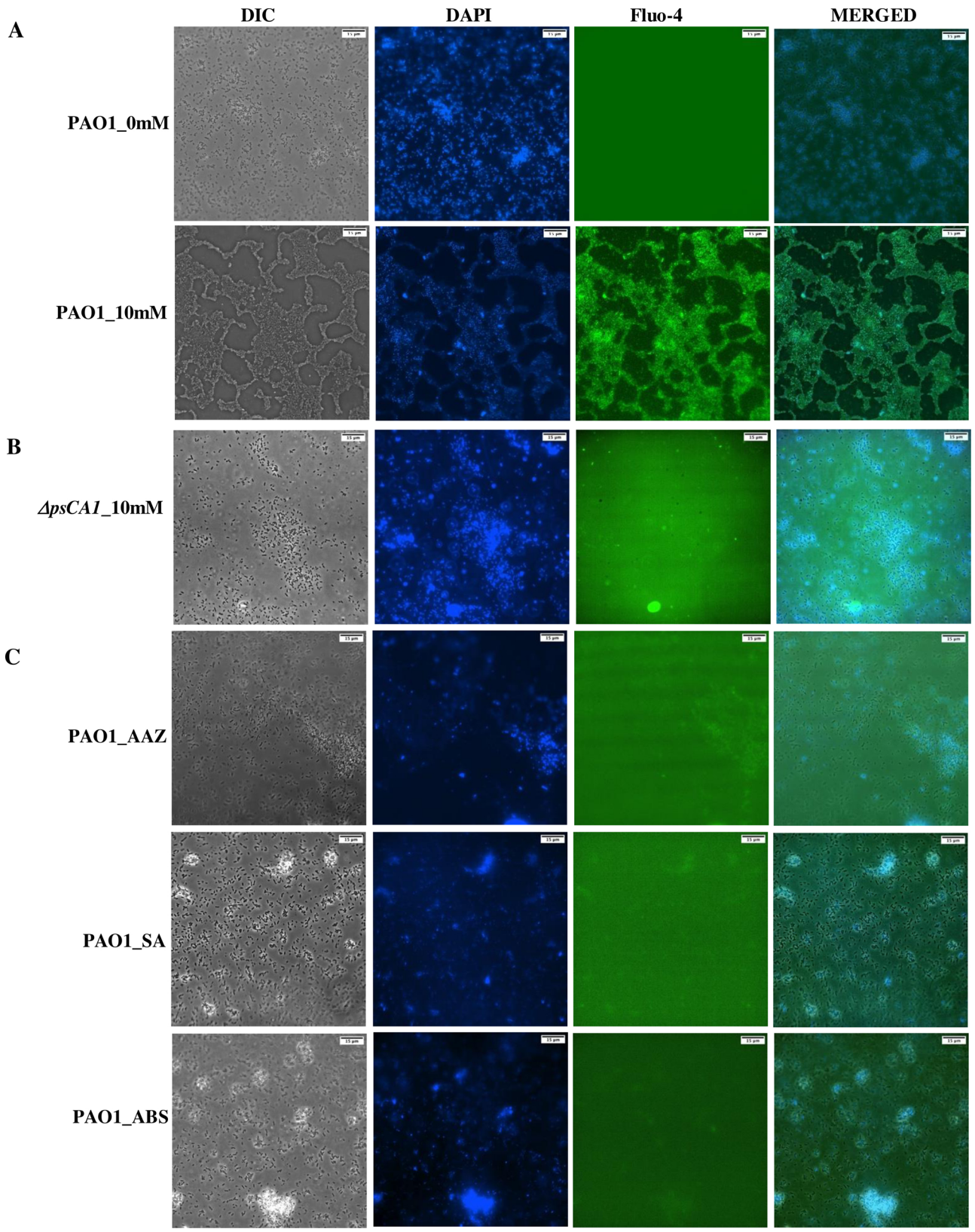

Fig. 3. Fluo-4 staining of calcium deposition in biofilms after 48 h by A. PAO1 grown at no added or 10 mM $CaCl_2$, B. Δ*psCA1* grown at 10 mM $CaCl_2$, C. PAO1 grown at 10 mM $CaCl_2$ in the presence of 100 μM of CA inhibitors: AZZ, SA, and ABS.

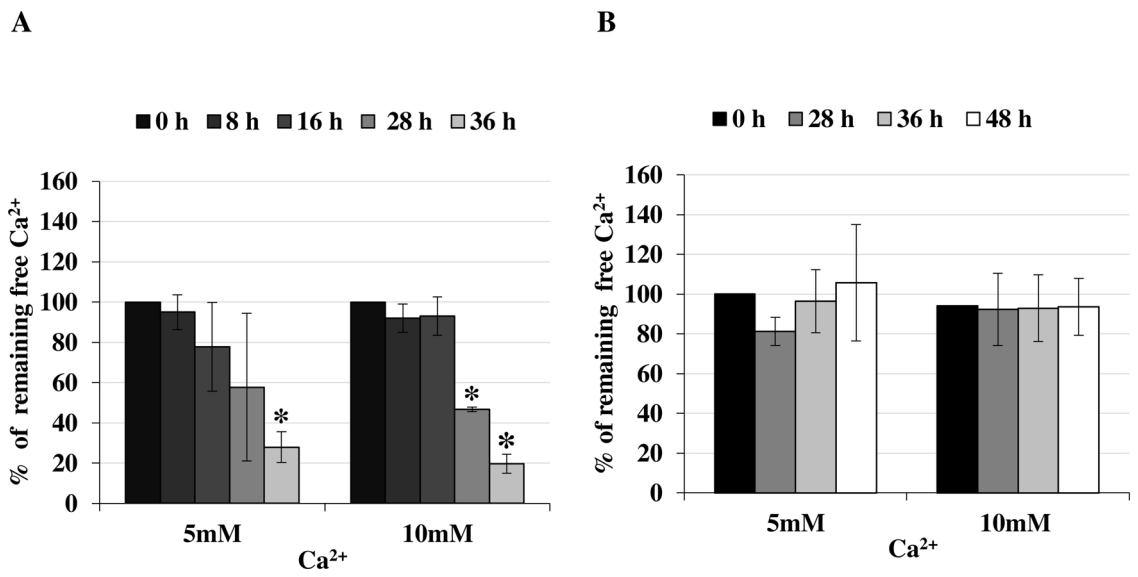

Fig. 4. Deposition of calcium by *P. aeruginosa* PAO1. Percentage of remaining free Ca^{2+} in the supernatants of PAO1 growth at: A. Static conditions, 5% CO_2 B. Shaking conditions, ambient CO_2. The symbol * represents statistically significant difference when compared to time 0 h (n = 3, P ≤ 0.05; paired t-test).

background (Fig. 3C)

3.6. Ca^{2+} regulates the expression of psCA1 in P. aeruginosa

In the previous studies, we showed that externally added Ca^{2+} alters the expression of a number of genes in *P. aeruginosa* [75]. We tested whether the abundance of psCA proteins is affected by elevated levels of Ca^{2+}. For this, immunoblot analysis of the protein extracts of PAO1 cells grown at 1 mM or 10 mM $CaCl_2$ was performed. His-tag purified psCA1, psCA2, and psCA3 were used as positive controls. All three proteins were detected in PAO1 cells as recognized by the primary antiserum raised against β-class Cab from *M. thermoautotrophicum* ΔH (Fig. 7A). The relative abundance of psCA1 appeared to be increased at 10 mM $CaCl_2$. The abundance of the other two psCAs did not appear altered. This increase in psCA1 abundance is in agreement with the earlier reported microarray analysis that showed seven-fold elevated expression of *psCA1* in response to 10 mM $CaCl_2$, but no changes in the expression of *psCA2* and *psCA3* (GEO dataset GSE74444). Further in agreement, RNA Seq analysis reported in (Guragain et.al. submitted for publication) showed that growth in the presence of 5 mM $CaCl_2$ increased the transcription of *psCA1* by 2-fold, whereas the transcription of *psCA2* and *psCA3* did not change. Here, we further validated the Ca^{2+} induction of *psCA1* expression by using RT-qPCR. The transcription of *psCA1* increased by about 5-fold in the cells grown at 5 mM $CaCl_2$ (Fig. 7B).

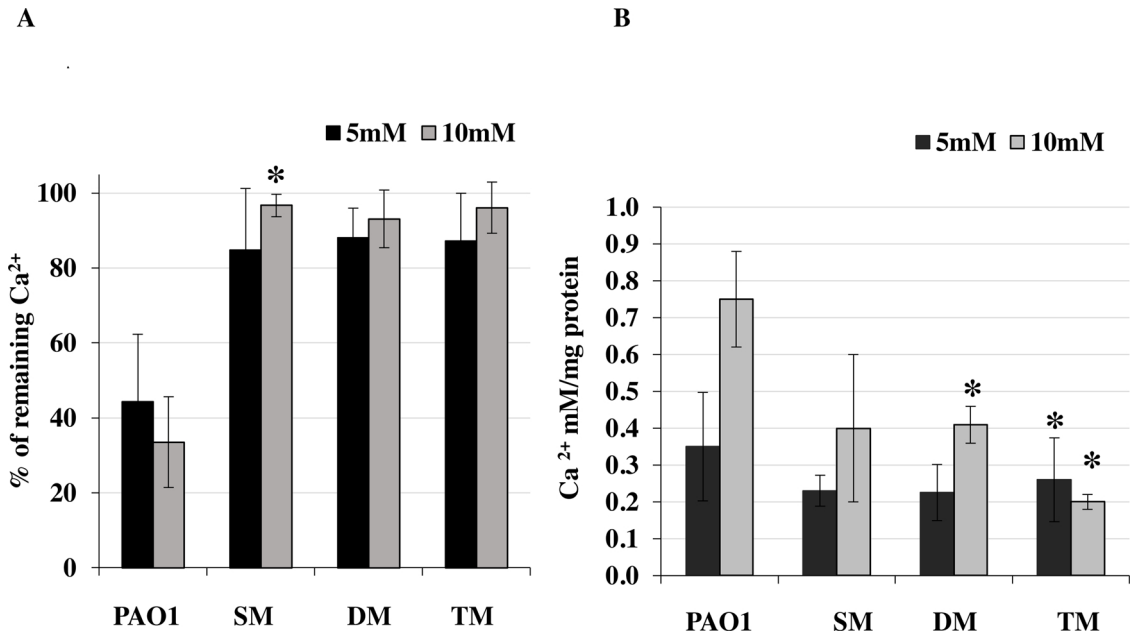

Fig. 5. Calcium deposition in *psCA* mutants. A. Percentage of remaining free Ca^{2+} in the supernatants after 48 h of incubation under static condition at 5% CO_2. B. Calcium deposited on glass walls after 48 h of incubation under static condition at 5% CO_2 in the presence of 5 mM or 10 mM $CaCl_2$. Calcium data were normalized by total cellular protein. The symbol * represents statistically significant difference when compared to wild type PAO1 grown at the corresponding condition (n = 3, P ≤ 0.05; paired t-test).

Table 3
Kinetic parameters for the CO_2 hydration reaction catalyzed by the β-CAs *Pseudomonas aeruginosa* psCA1 (shown in bold), *C. neoformans* Can2, *C. albicans* CalCA, *S. cerevisiae* SceCA, *Flaveria bidentis* FbiCA1 and CahB1, *Helicobacter pylori* hpβCA measured at 20 °C, pH 8.3 in 20 mM TRIS buffer and 20 mM NaClO. as well as human cytosolic isozymes hCA I and II (α-class CAs) measured at 20 °C and pH 7.5 in 10 mM HEPES buffer and 20 mM Na_2SO_4. Measurements for *H. pylori* hpαCA were carried out at pH 8.9 and 25 °C. Inhibition data with the clinically used sulfonamide acetazolamide (5-acetamido-1,3,4-thiadiazole-2-sulfonamide) are also provided (stopped-flow assay).

Enzyme	k_{cat} (s^{-1})	k_{cat}/K_m (M^{-1}x s^{-1})	Activity level
hCA I	2.0×10^5	5.0×10^7	moderate
hCA II	1.4×10^6	1.5×10^8	very high
Can2	3.9×10^5	4.3×10^7	moderate
CalCA	8.0×10^5	9.8×10^7	high
SceCA	9.4×10^5	9.8×10^7	high
FbiCA 1	1.2×10^5	7.5×10^6	low
CahB1	2.4×10^5	6.3×10^7	moderate
psCA1	$\mathbf{1.8 \times 10^5}$	$\mathbf{7.5 \times 10^7}$	**moderate**
hpαCA[117]	2.5×10^5	1.5×10^7	low
hpβCA[117]	7.1×10^5	4.8×10^7	medium

Table 4
Inhibition constants of anionic inhibitors against *P. aeruginosa* psCA1 and the α-CA (human) isoform hCAII for the CO_2 hydration reaction, measured at 20 °C and pH 8.3.

Inhibitor	K_I [mM][#]	
	hCA II [a]	psCA1[c]
F^-	> 100	> 100
Cl^-	> 100	> 100
Br^-	63	> 100
I^-	26	> 100
CNO^-	0.03	0.58
SCN^-	1.6	0.76
CN^-	0.02	0.84
N_3^-	1.5	12.5
HCO_3^-	85	3.5
CO_3^{2-}	73	1.4
NO_3^-	35	8.9
NO_2^-	63	0.91
HS^-	0.04	0.91
HSO_3^-	89	5.3
$SO4^{2-}$	> 100	> 100
SnO_3^{2-}	0.83	0.61
SeO_4^{2-}	112	0.91
TeO_4^{2-}	0.92	2.3
$P_2O_7^{4-}$	48.50	6.2
$V_2O_7^{4-}$	0.57	1.9
$B_4O_7^{2-}$	0.95	4.5
ReO_4^-	0.75	4.4
RuO_4^-	0.69	2.9
$S_2O_8^{2-}$	0.084	> 100
$SeCN^-$	0.086	7.2
CS_3^{2-}	0.0088	5.1
$Et_2NCS_2^-$	3.1	0.77
ClO_4^-	> 100	> 100
BF_4^-	> 100	> 100
FSO_3^-	0.46	> 100
$NH(SO_3)_2^{2-}$	0.76	> 100
$H_2NSO_2NH_2$ (SA)	**1.13**	**0.009**
H_2NSO_3H	**0.39**	**0.080**
Ph-$B(OH)_2$	**23.1**	**0.037**
Ph-AsO_3H_2	**49.2**	**0.070**
PF_6^-	NT	8.4

[#] Errors were in the range of 3–5 % of the reported values, from three different assays.
[a] Human recombinant isozyme, stopped flow CO_2 hydrase assay method, from ref.[117].
[c] Recombinant enzyme, this work.
NT, not tested.

Table 5
Inhibition constants of sulfonamides (1–24) and the clinically used drugs (AAZ – HCT) tested against *P. aeruginosa* psCA1 and the α-CA (human) isoform hCAII for the CO_2 hydration reaction, measured at 20 °C and pH 8.3.

	K_I* (nM)			
Inhibitor/Enzyme class	hCA II[a]	psCA1[c]	hpαCA	hpβCA
1 (ABS)	300	19	426	16400 ± 820
2	240	86	454	1845 ± 54
3	8	39	316	8650 ± 62
4	20	78	430	2470 ± 104
5	170	84	873	2360 ± 170
6	160	67	1150	3500 ± 61
7	60	79	1230	1359 ± 37
8	110	483	378	1463 ± 55
9	40	554	452	1235 ± 60
10	54	> 20000	510	1146 ± 29
11	63	> 20000	412	973 ± 36
12	75	> 20000	49	640 ± 18
13	60	88	323	2590 ± 74
14	19	403	549	768 ± 38
15	80	741	268	64 ± 5
16	94	588	131	87 ± 7
17	125	> 20000	114	71 ± 3
18	46	> 20000	84	38 ± 2
19	33	> 20000	207	39 ± 3
20	2	753	105	37 ± 2
21	11	78	876	236 ± 19
22	46	> 20000	1134	218 ± 16
23	33	> 20000	1052	450 ± 27
24	30	694	541	15250 ± 605
AAZ	12	37	21	40 ± 3
MZA	14	46	225	176 ± 12
EZA	8	32	193	33 ± 1
DZA	9	38	4360	73 ± 7
BRZ	3	66	210	128 ± 11
BZA	9	76	315	54 ± 4
TPM	10	> 20000	172	32 ± 2
ZNS	35	837	231	254 ± 18
SLP	40	310	204	35 ± 3
IND	15	225	413	143 ± 14
VLX	43	> 20000		
CLX	21	757		
SLT	9	9 905		
SAC	5959	907		
HCT	290	> 20000		

* Errors in the range of 5–10 % of the shown data, from 3 different assays.
[a] Human recombinant isozyme, stopped flow CO_2 hydrase assay method[117].
[c] Recombinant enzyme, this work.
1, 3-amino-benzene sulphonamide; 2, 4-amino-benzene sulfonamide (sulfanilamide); 3, benzene-1,3-disulfonamide; 4, 4-toleune sulphonamide; 5, 4-(aminomethyl)-benzene sulphonamide; 6, 4-(2-aminoethyl)-benzene sulphonamide; 7, 3-fluoro-4-amino-benzene sulphonamide; 8, 3-chloro-4-amino-benzene sulphonamide; 9, 4-amino-3-bromo-benzene sulphonamide; 10, 3,5-dichloro-2-hydroxy-benzene sulphonamide; 11, 4-amino-6-trifluoromethyl-benzene 1,3-disulfonamide; 12, 4-amino-6-chlorobenzene-1, 3-disulfonamide; 13, 5-amino-1, 3,4-thiadiazole-2-sulfonamide; 14, 5-Imino-4-methyl-1, 3,4-thiadiazole-2-sulfonamide; 15, 4-hydroxy-benzene sulphonamide; 16, 4-hydroxy-methyl-benzene sulphonamide; 17, 4-hydroxy-ethyl-benzene sulphonamide; 18, 4-carboxy-benzene sulfonamide; 19, 4-((2-amino-4-pyrimidinyl)amino)-benzene sulfonamide; 20, 5-(sulfanilamido-1, 3, 4-thiadiazole-2-amino sulphonamide; 21, 2-(hydroxymethyl)-4-nitro-N-(4-sulfamoylphenylethyl) benzene sulfonamide; 22, 4-amino-N-(4-sulfamoylphenyl) benzene sulfonamide; 23, 4-amino-N-(4-sulfamoylbenzyl) benzene sulfonamide; 24, 4-amino-N-(4-sulfamoylphenethyl) benzene sulfonamide.
AAZ, Acetazolamide; MZA, Methazolamide; EZA, Ethoxzolamide; DCP, Dichlorphenamide; DZA, Dorzolamide; BRZ, Brinzolamide; BZA, Benzolamide; TPM, Topiramate; ZNS, Zonisamade; SLP, Sulpiride; IND, Indisulam; VLX, Valdecozib; CLX, Celecoxib; SLT, Sulthiame; SAC, Saccharin; HCT, Hydrochlorothiazide.

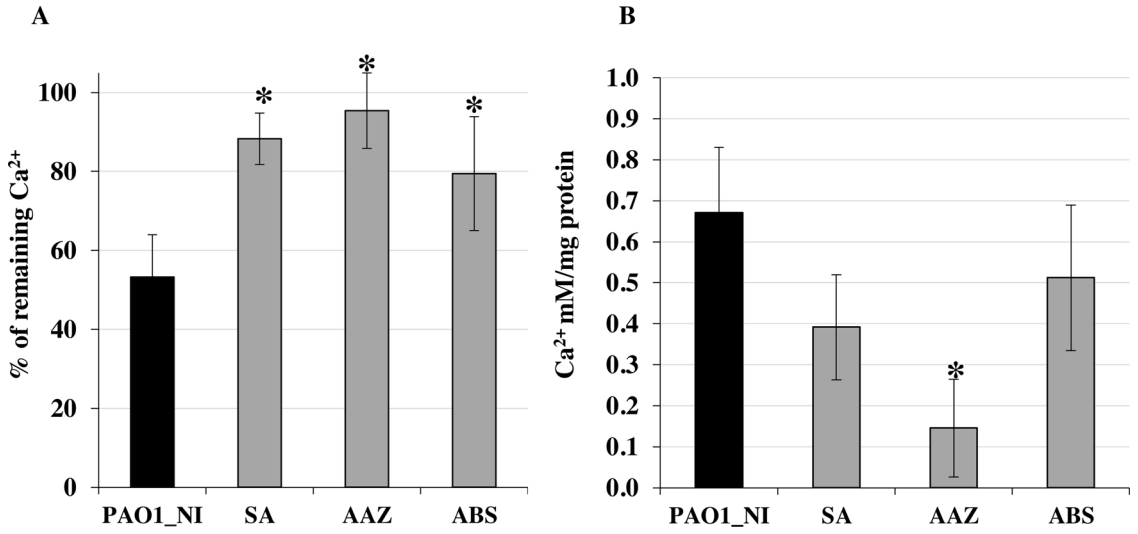

Fig. 6. The effect of CA inhibitors SA, AAZ, and ABS on calcium deposition of *P. aeruginosa* PAO1. PAO1_NI is wild type PAO1 grown in the absence of inhibitors. A. Percentage of remaining free Ca^{2+} in the supernatants after 48 h of incubation under static condition at 5% CO_2. B. Calcium deposited on glass walls during 48 h of growth in BMM with 10 mM $CaCl_2$ under static condition at 5% CO_2. Calcium data were normalized by total cellular protein. The symbol * represents statistically significant difference when compared to wild type PAO1 grown in the absence of inhibitors (n = 3, P ≤ 0.05; paired t-test).

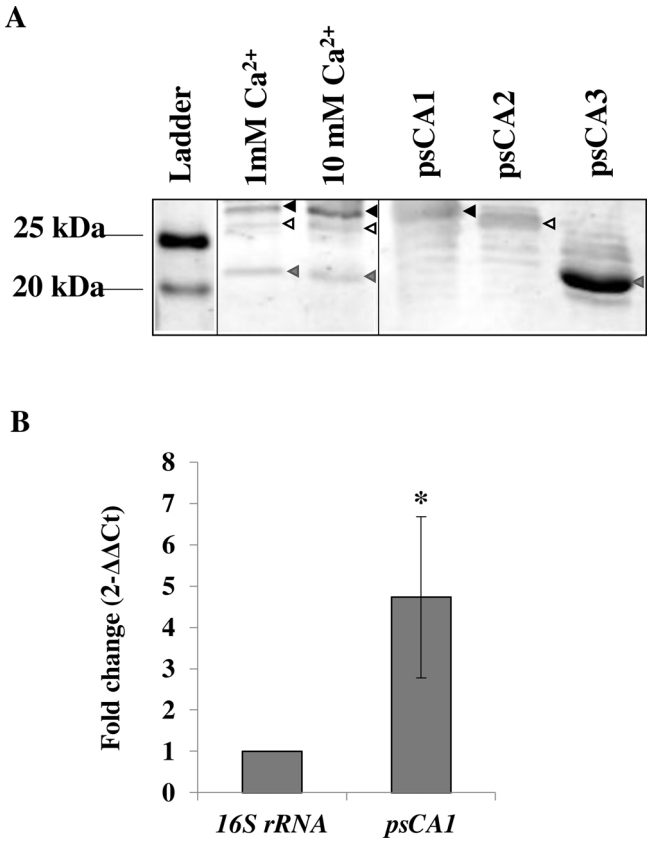

Fig. 7. Regulation of *psCA1* by Ca^{2+}. A. Immunoblot analysis of the protein extracts of PAO1 cells grown at no added, or 1 mM, or 10 mM $CaCl_2$. Purified His-tag CAs psCA1, psCA2, and psCA3 were used as positive controls. Primary antiserum raised against β-class Cab from *M. thermoautotrophicum* ΔH was used to detect the proteins. B. RT-PCR using primers designed to examine transcriptional response of *psCA1* to 5 mM Ca^{2+}. The housekeeping gene *16SrRNA* was selected as an experimental control since its transcriptional response was not affected by the presence of Ca^{2+}. The symbol * represents statistically significant difference when compared to the change in transcript abundance of the housekeeping gene *16SrRNA* (n = 3, P ≤ 0.05; paired t-test).

3.7. β-CA psCA1 contributes to P. aeruginosa virulence at elevated levels of Ca^{2+} ions

We hypothesized that the ability of *P. aeruginosa* to deposit calcium enhances virulence of the pathogen and that the deletion of *psCA1* would have a negative impact. This was tested by using *Galleria mellonella* (wax worms) infection model. Indeed, we observed that when wild type *P. aeruginosa* was grown and injected at no added $CaCl_2$ with the infection doze of 2–3 CFU, only 10% of the worms were killed after 20 h of incubation (Fig. 8A, black line). However, either increasing the infection doze to 6–11 CFU or growing and injecting bacteria in the presence of 10 mM $CaCl_2$ decreased the survival to 60–80 % (Fig. 8B, C, black line). Furthermore, infecting larvae with the higher doze of the pathogen grown at 10 mM $CaCl_2$ further decreased the survival to 20% (Fig. 8D, black line). These observations supported the inducing effect of Ca^{2+} on *P. aeruginosa* virulence. To make sure that the injected *P. aeruginosa* cells were exposed to elevated levels of Ca^{2+} while within the larvae, we have monitored the level of free Ca^{2+} in the hemolymph samples collected from the injected worms. When bacteria were injected in the presence of 10 mM of $CaCl_2$, the level of free Ca^{2+} in the collected larva hemolymph 10 h post infection (hpi) was 7.8 +/- 0.2 mM, whereas after infecting *P. aeruginosa* grown at no added $CaCl_2$, the concentration of Ca^{2+} was 3.8 +/- 0.3 mM. In contrast to the wild type, no killing was observed after infecting with the *ΔpsCA1* mutant under the conditions tested after 20 h of incubation (Fig. 8, dark grey line). We have also tested whether the presence of 100 μM AAZ would impact *P.aeruginosa* virulence by inhibiting the activity of psCA1. However, no significant difference was observed (data not shown).

3.8. Active site differences between psCA1, psCA2, and psCA3

A structural characterization was done to compare the active sites of psCA3 X-ray crystal structure [48] and *in-silico* models of psCA1 and psCA2 (Fig. 8). Superposition of the three structures resulted in very similar α-carbon root mean square deviation (rmsd) values, indicating that the overall three-dimensional structures are essentially the same. The rmsd of psCA1 and psCA2 to psCA3 were 0.26 and 0.20 Å, respectively, with the sequence identities being ~30% for both enzymes. The rmsd between the psCA1 and psCA2 models was 0.33 Å. Despite the overall structural similarity there were three solvent accessible loops (regions 1,2 and 3) of the structure where the psCA1 was unique

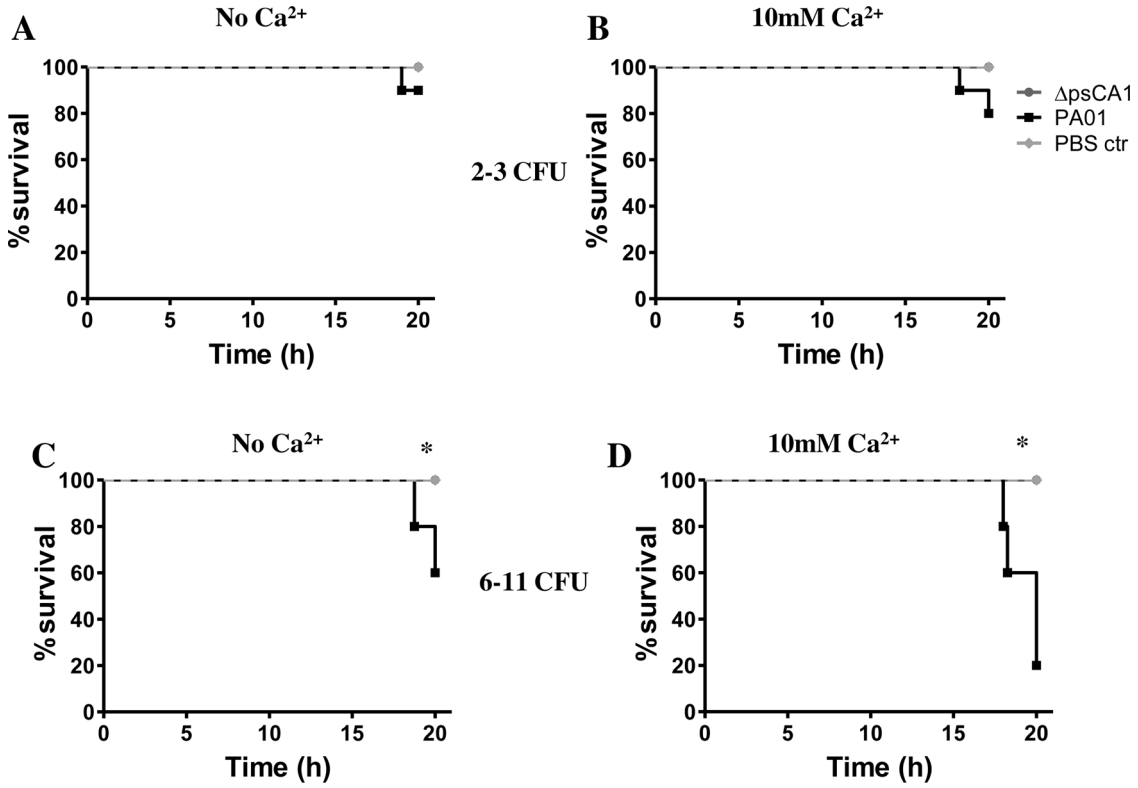

Fig. 8. Virulence assay in *Galleria melonella* (wax worm) infection model. Killing curves of wax worm larvae inoculated with PAO1 and Δ*psCA1* cultures grown in BMM without added $CaCl_2$ (A, C) or supplemented with 10 mM $CaCl_2$ (B, D). The injections were administered with low dose of 2–3 CFU (A, B) or high dose of 6–11 CFU (C, D). The symbol * represents statistically significant difference (n = 10, P ≤ 0.05; Log-rank test in Prism).

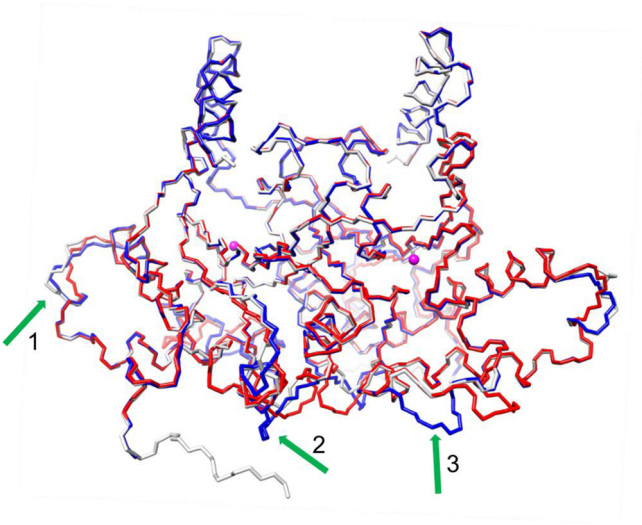

Fig. 9. Structural comparison of psCA1, psCA2, and psCA3. Depicted main-chain fold, overlay of dimeric psCA1 (blue), psCA2 (red), psCA3 (grey). The green arrows denote three regions that differ between the structures. Region 1 – deletion of an amino acid, region 2 and 3 – insertion of amino acids into the structure of psCA1, compared to psCA2 and 3.

compared to psCA2 and psCA3 (Fig. 9, green arrows). In region 1, there is a single amino acid insertion, between G161 and A162 (psCA1 numbering) in psCA3. In addition to the amino acid deletion, there is also a conformational loop shift between amino acids 158 and 163 (psCA1: CDCGA, psCA2: HAS (also has deletions), psCA3: EQLPT). Region 2, is where the most conformational variation between the structures is observed, here there is a loop insertion between amino acids 90–93 in psCA1 and psCA2 that is not present in psCA3. This insertion again lends to structural perturbations in the region. Finally, in region 3 there is a three amino acid insertion between residues 133 and 137 for psCA1 and a three amino acid insertion between residues 131 and 135 in psCA2. Any one of these surface conformational changes between the three enzymes may affect their recognition of other cellular factors.

In addition to these surface loop conformational differences, the active sites of each of the psCAs exhibited unique amino acids proximal to the CO_2 binding site [76]. In particular psCA1, had four active site amino acids that differed from psCA2 and 3 (Fig. 9 insert; 59 T, 61A, 101A, and 108A), and these differences would most definitely have effects on the catalytic activity. Also noteworthy, was the observation, that most of the amino acids that line the secondary CO_2 binding site [76], at the dimer interface, differed in psCA1 compared to psCA2 and 3 (Fig. 9 insert 2C, 59 T, 61A, and 81 T) which may also have a role in effecting calcium salt deposition.

4. Discussion

Soft tissue calcification is a consequential medical condition causing a number of human diseases, however its molecular origins are not well defined. Since soft tissue calcification can be associated with bacterial infections, we hypothesized that a human pathogen *P. aeruginosa* is capable of initiating deposition of calcium, and that its CAs contribute to this process. For the first time, this study identified the ability of *P. aeruginosa* PAO1 to form calcium-containing deposits and elucidated the role of β-CA psCA1 in the formation of calcium deposits and virulence of the pathogen. We also identified several inhibitors of the enzyme at micro and nano-molar levels and performed *in-silico* structural analysis. We provide the first evidence that inhibiting the CA activity in *P. aeruginosa* significantly reduces its ability to deposit calcium, which may impact physiology and virulence of the pathogen.

Bacteria-driven mineralization of $CaCO_3$ may occur due to urease or

CA activity [77]. CAs enable sequestering CO_2 by conversion to bicarbonate, which in the presence of Ca^{2+} precipitate as $CaCO_3$. Several bacteria including *P. aeruginosa*, have been associated with formation of $CaCO_3$ deposits [25,28,78–80]. Calcite biomineralization by *P. aeruginosa* biofilms has been detected at high levels of Ca^{2+} (15 mM) and shown to impact biofilm architecture [79]. However, the molecular mechanisms have not been studied in detail. Here, we observed that *P. aeruginosa* deposits calcium and showed that this deposition occurs in the presence of 5–10 mM $CaCl_2$ and is favored at non-shaking conditions with 5% CO_2. After 36–48 h of growth under these conditions, free Ca^{2+} in cell cultures was reduced significantly, and higher levels of calcium deposition on the glass walls were detected. In contrast, there was almost no calcium deposition during growth under shaking conditions and ambient CO_2. This indicated that providing more CO_2 and allowing cells to settle on a surface supports calcium deposition. It is important to note that such conditions are prevalent in human bacterial infections.

Previously, we reported the identification of three functional β-CAs in *P. aeruginosa* and showed that one of them, psCA1, has the highest CO_2-hydrating activity and plays role in survival of the organism in ambient air [47]. However, the role of these enzymes in calcium deposition had not been studied. Here, we show that calcium deposition by *P. aeruginosa* PAO1 requires CA activity, and psCA1 is the main contributor to this process. In support of our earlier data, we also observed that under shaking conditions with ambient CO_2, single, double, and triple mutants lacking β-CAs, showed a proportional growth delay, which was not apparent under static conditions with 5% CO_2. This most likely reflects that providing 5% CO_2 satisfies the needs of *P. aeruginosa* in bicarbonate for C1 metabolism, the products of which feed into anabolic reactions [81]. Similarly, in *E. coli,* the β-class CA, Can, is essential for growth at low partial pressure of CO_2, but dispensable at elevated CO_2 [82]. We also showed that calcium deposition requires and is proportional to the levels of free Ca^{2+} initially present in the medium. *P. aeruginosa* almost doubled the amount of deposited calcium at 10 versus 5 mM of added $CaCl_2$ in the medium (Fig. 5B). This observation is of clinical significance since the levels of Ca^{2+} can be elevated in body fluids and tissues during certain human diseases. For example, sputum, pulmonary fluid and nasal secretions in patients with cystic fibrosis [83–85], urine in patients with post-glomerular hematuria [86], and blood in some cases of tuberculosis [87] contain elevated levels of Ca^{2+}.

The three β−CAs in *P. aeruginosa* share 28–45% amino acid sequence identity, and are encoded within different genetic neighborhoods [47]. This suggests differences in their regulation and physiological roles. Among them, the most active psCA1 showed the highest abundance under the tested growth conditions [47]. It is encoded within a putative operon with permease PA0103 that belongs to a major facilitator superfamily (MFS), some members of which are known to transport bicarbonate [88]. Thus, PA0103 may be involved in translocation of HCO_3^- from the cytosol into the environment where it is converted to carbonate and forms $CaCO_3$, which precipitates upon accumulation. Similarly, the Ca^{2+}-dependent HCO_3^- transporter, BCT1, from *Synechocystis* sp. PCC 6803 was shown to be involved in precipitation of $CaCO_3$ [26]. A second *P. aeruginosa* β-CA, encoded by *psCA2,* is 65% identical to the CynT from *E. coli* and is clustered with *cynS,* a cyanate lyase and a transcriptional regulator, *cynR*. In *E. coli*, a homologous cyanate lyase CynS catalyzes the conversion of cyanate into ammonia and CO_2 [89,90]. Thus, psCA2 likely catalyzes the hydration of CO_2 generated by CynS. Therefore, psCA2 may potentially also contribute to calcium deposition, but requires the presence of cyanate. Finally, a third β-CA in PAO1, psCA3, showed a low CO_2 hydration activity [47]. Its encoding gene is clustered with a predicted peptidase (PA4677) and TonB receptor (PA4675), and may be functionally related to protein modification or degradation. The relation of this CA with other metabolic processes in not clear and requires further studies.

Our *in-silico* modeling (Figs. 9 & 10) has confirmed the overall structural conservation between the three *P. aeruginosa* β-CAs, yet it also highlights conformation differences in surface loop regions, that may contribute to their recognition of other (currently unknown) cellular factors. Understanding how these loops modulate their function may further our understanding for why all three are expressed. Also, the unique amino acids proximal to the CO_2 binding site (T59, A61, A101, and A108, psCA1 numbering), and the secondary CO_2 binding site at the dimer interface (C2, T59, A61, and T81, psCA1 numbering) would most definitely have effects on the catalytic activity and modulate the effectiveness of inhibitor design. Therefore, they may affect the role of the enzymes in calcium deposition and cell physiology.

Previously, we showed that elevated CO_2 leads to increased abundance of psCA1 and significantly lower level of psCA3 [47]. A similar induction of biosynthesis of Nce103, CA in *Saccharomyces cerevisiae,* was observed in response to lower CO_2 [91]. This supports the role of psCA3 in overcoming a lack of C1 compounds under this condition. On the other hand, a slight increase of psCA1 abundance at higher CO_2 [47] together with the Ca^{2+}-induction of *psCA1* expression reported here support the role of this protein in calcium deposition, which requires both elevated CO_2 and Ca^{2+}. This also indicates that the ability of *P. aeruginosa* to deposit calcium is regulated by the cation at the transcriptional level, suggesting the presence of transcriptional regulators recognizing Ca^{2+} fluctuations. Further studies will address this question.

Microscopy studies showed that *P. aeruginosa* appears to form oval-shaped calcium deposits in cell cultures (Fig. 2) and harbor Ca^{2+} on the cell surfaces (Fig. 3). It is possible that calcium deposition is initiated at cell surface, where Ca^{2+} binding is promoted by the presence of negatively charged groups of lipopolysaccharides, for example [92]. This Ca^{2+} binding may foster nucleation, a key physical parameter required for initiating calcium mineralization [20,23,93].

The phenomenon of CAs-mediated $CaCO_3$ precipitation in *P. aeruginosa* may have multiple implications in natural environments and clinical settings. As an environmental organism, *P. aeruginosa* may contribute to CO_2 sequestration reducing atmospheric levels of CO_2 as was described for *Citrobacter freundii* and *Bacillus subtilis* [94,95]. As a human pathogen, *P. aeruginosa* may contribute to soft tissue calcification or stone formation during infectious process. Calcium rich deposits have been found in the lungs of primary ciliary dyskinesia [96], cystic fibrosis [97] and infective endocarditis [98] which could be related to the activity of *P. aeruginosa* commonly associated with these diseases. *P. aeruginosa* is one of the pathogens associated with the infections in catheterized urinary tracts [99] and may contribute to the biomineralization of $CaCO_3$ leading to encrustation of catheters [99–101]. Moreover, $CaCO_3$ deposition may initiate the formation of kidney and bladder stones [102–104] or promote the crystallization of calcium oxalate, the major constituent of most urinary stones [105].

Our data showed that the presence of elevated Ca^{2+} enhanced virulence of *P. aeruginosa* when tested using *G. melonella* as an infection model. This agrees with the previously observed Ca^{2+}-induced virulence of the pathogen in lettuce leaves [106]. The impact may due to a combination of factors, including the earlier reported virulence factors induced by Ca^{2+}, such as secreted proteases and pyocyanin [50]. It may also be further enhanced by the ability to deposit calcium, which can be considered as a novel virulence factor of *P. aeruginosa*. The latter is supported by the reduction in virulence in the mutant lacking *psCA1* (Fig. 8). However, considering that the effect was also observed at no added Ca^{2+}, this enzyme may have additional role(s) in the pathogen's virulence.

According to the microarray expression data available in NCBI, the transcription of *psCA1* and *psCA2* was induced at least threefold in *P. aeruginosa* isolates from CF lung sputa (GDS2869) [107], the transcription of *psCA1* increased fourfold in burn wound model and ninefold in *P. aeruginosa* isolates from CF sputum (GDS2869) [108]. This increased expression in clinical conditions supports a role of these

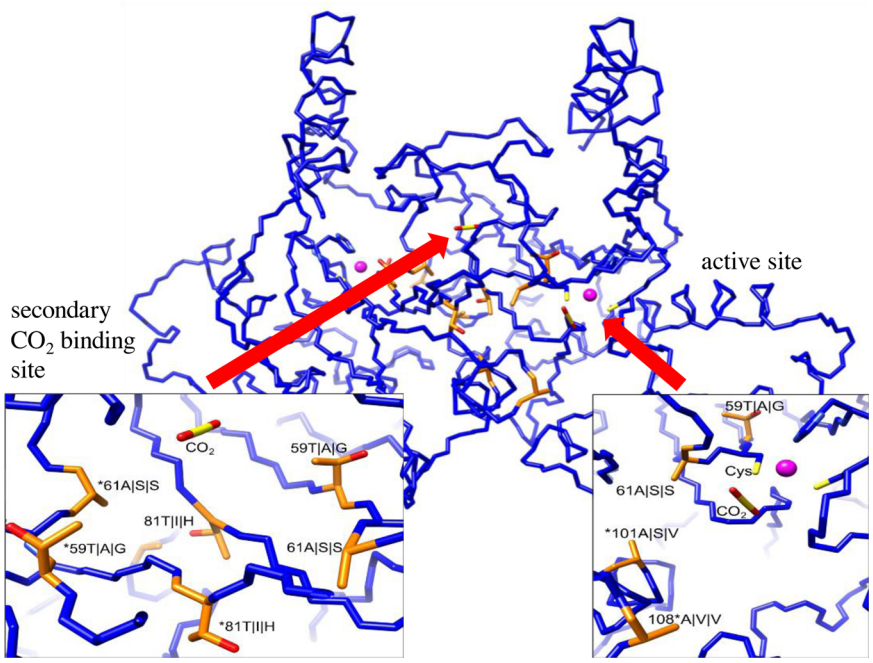

Fig. 10. Structure of psCA1. Highlighting amino acids unique to psCA1 compared to psCA2 and 3. Insert boxes highlight psCA1 active site and secondary CO_2 binding site. Amino acids unique to psCA1 are depicted in orange, CO_2 molecules are shown in yellow, and zinc ions in magenta. Amino acids are as labeled; residue number (psCA1 numbering), then amino acid type for psCA1, 2, and 3, respectively. *denotes dimer related amino acid.

proteins during *P. aeruginosa* infections, potentially enabling the pathogen's survival in a host, as it has been shown for other bacterial β-CAs. The examples include a macrophage-induced β-CA, stCA1 (previously known as Mig-5) from *Salmonella typhimurium* [40,109–111], Rv1284 and Rv3385c from *Mycobacterium tuberculosis* [112–114],and Pca from *Streptococcus pneumoniae* are essential for survival inside the host cells [115]. Nce103 from *Candida albicans* is essential for the pathogen's survival in the host microenvironments with limited supply of CO_2 [116], and *Helicobacter pylori* hpβCA as well as α-class hpαCA enable the pathogen's survival in the highly acidic conditions of the stomach [117–119]. Further studies are needed to decipher the role of $CaCO_3$ precipitation in virulence and pathogenicity of *P. aeruginosa* as well as other pathogenic bacteria, many of which contain multiple β-CAs as well as α and γ-CAs.

Beta-CAs are prevalent in bacteria, fungi, and algae. They present a promising target for developing specific inhibitor due to the lack of β-CAs in humans and no similarity between bacterial β-CAs and human α−CAs. Inhibition of β-CAs has been reported to attenuate virulence and growth in *M. tuberculosis*, *H. pylori, and Brucella spp.* For example, inhibition of *Brucella* expressing bsCA II by 100 μM of acetazolamide, glycosylsulfonamide and sulfamates resulted in growth delay [120]. Treating *M. tuberculosis* producing three β-CAs, mtCA1, mtCA2 and mtCA3, with 80 μM of ethoxzolamide (EZA), a sulfonamide derivative, showed a significant inhibition of growth in macrophages through downregulation of PhoPR two component system and its regulon [114]. The latter is required for intracellular growth and replication of *M. tuberculosis* and is induced by acidic pH in the macrophages [121]. Several β-CAs, including mtCA1 from *M. tuberculosis* [122], hpβCA from *H. pylori* [117], stCA1 and stCA2 from *S. typhimurium* [111], have been studied as targets of sulfonamides in attempts of developing therapeutics. The results of these studies present the inhibition of β-CA as a potentially successful alternative for managing diseases such as gastric ulcer, gastritis, and tuberculosis. Here, we have identified several molecules that inhibit psCA1 at nano- to micro-molar level. Our results showed that adding 100 μM of AAZ, SA, or ABS had a drastic negative impact on calcium deposition in *P. aeruginosa.* Previously, we showed that AAZ also delayed planktonic growth of the pathogen at ambient air [47]. However, AAZ has been shown to have inhibiting impact on eukaryotic CA-driven calcification, for example, in the sponge *Sycon raphanus* [123] and in human osteogenic cells [124]. Therefore, there is a need in developing further more powerful and specific inhibitors that would control the ability of *P. aeruginosa* to deposit calcium and thus enhance the chances of treating its deadly infections.

Acknowledgements

This work was supported by the Research grant from OCAST (Award#HR12-167). We thank Dr. James Ferry (Pennsylvania State University) for providing primary antiserum. TEM and EDX analysis were performed by Lisa Whitworth at the Microscopy facility at Oklahoma State University (OSU). Fluorescent microscopy was performed in Dr. Randy Morgenstein's laboratory at OSU.

Appendix A. Supplementary data

Supplementary material related to this article can be found, in the online version, at doi:https://doi.org/10.1016/j.ceca.2019.102080.

References

[1] J.D. Hutcheson, et al., Revisiting cardiovascular calcification: a multifaceted disease requiring a multidisciplinary approach, Semin. Cell Dev. Biol. (2015).
[2] W. Gamble, Atherosclerosis: the carbonic anhydrase, carbon dioxide, calcium concerted theory, J. Theor. Biol. 239 (1) (2006) 16–21.
[3] G. Halmerbauer, et al., The relationship of eosinophil granule proteins to ions in the sputum of patients with cystic fibrosis, Clin. Exp. Allergy 30 (12) (2000) 1771–1776.
[4] M.I. Lorin, G.P, I.D. Mandel, C.R. Denning, Composition of nasal secretion in patients with cystic fibrosis, J. Lab. Clin. Med. 88 (1) (1976) 114–117.
[5] C. Sabanayagam, S.A, Serum calcium levels and hypertension among U.S. adults, J. Clin. Hypertens. 13 (10) (2011) 716–721.
[6] J.S. Rolf Jorde, Patrick Fitzgerald, Kaare H. Bønaa, Serum calcium and cardiovascular risk factors and diseases: the Tromsø study, Hypertension 34 (1999) 484–490.
[7] L. Gilardini, et al., Factors associated with early atherosclerosis and arterial calcifications in young subjects with a benign phenotype of obesity, Obesity 19 (8) (2011) 1684–1689.
[8] C.M. Shanahan, et al., Arterial calcification in chronic kidney disease: key roles for calcium and phosphate, Circ. Res. 109 (6) (2011) 697–711.
[9] I. Kholová, et al., Lymphatic vasculature is increased in heart valves, ischaemic and inflamed hearts and in cholesterol-rich and calcified atherosclerotic lesions, Eur. J. Clin. Invest. 41 (5) (2011) 487–497.
[10] K.N. Naruhiko Ishiwada, Shigeru Tateno, Masao Yoshinaga, M.N. Masaru Terai, Causative organism influences clinical profile and outcome of infective endocarditis in pediatric patients and adults with congenital heart disease, Circ. J. 69 (2005) 1266–1270.

[11] A.A. Von Ruecker, Rosemarie Bertele, H. Karsten Harms, Calcium metabolism and cystic fibrosis: mitochondrial abnormalities suggest a modification of the mitochondrial membrane, Pediatr. Res. 18 (7) (1984) 594–599.
[12] G. Minardi, et al., Infective endocarditis on mitral annular calcification: a case report, Cases J. 2 (1) (2009) 9072.
[13] P.K. Shah, Link between infection and atherosclerosis. Who are the culprits: viruses, bacteria, both, or neither? Circulation 102 (2000) 2335–2340.
[14] V.L. Stewart, P. Herling, M.K. Dalinka, Calcification in soft tissues, JAMA 250 (1) (1983) 78–81.
[15] A.S. Black, K.I, A review of soft tissue calcifications, J. Foot Surg. 24 (4) (1985) 243–250.
[16] J.G. Ojemann, et al., Calcium carbonate apatite deposition in the cervical spine with associated vertebral destruction, J. Neurosurg. 86 (6) (1997) 1022–1026.
[17] W.E. Keefe, Formation of crystalline deposits by several genera of the family Enterobacteriaceae, Infect. Immun. 14 (2) (1976) 590–592.
[18] C. Rodriguez-Navarro, et al., Influence of substrate mineralogy on bacterial mineralization of calcium carbonate: implications for stone conservation, Appl. Environ. Microbiol. 78 (11) (2012) 4017–4029.
[19] F. Hammes, W. Verstraete, Key roles of pH and calcium metabolism in microbial carbonate precipitation, Rev. Environ. Sci. Biotechnol. 1 (1) (2002) 3–7.
[20] D. Fortin, F.G. Ferris, T.J. Beveridge, Surface-mediated mineral development by bacteria, Rev. Mineral. Geochem. 35 (1997) 161–180.
[21] S. Castanier, G. Le Métayer-Levrel, J.-P. Jean-Pierre Perthuisot, Ca-carbonates precipitation and limestone genesis — the microbiogeologist point of view, Sediment. Geol. 126 (1999) 9–23.
[22] S. Castanier, et al., O. Ciferri, P. Tiano, G. Mastromei (Eds.), Bacterial Carbonatogenesis and Applications to Preservation and Restoration of Historic Property, in Of Microbes and Art, Springer US, 2000, pp. 203–218.
[23] S. Douglas, T.J. Beveridge, Mineral formation by bacteria in natural microbial communities, FEMS Microbiol. Ecol. 26 (1998) 79–88.
[24] M. RY, Calcite precipitation by marine bacteria, Geomicrobiol. J. 2 (1980) 63–82.
[25] E.D. Banks, N.M. Taylor, J. Gulley, B.R. Lubbers, J.G. Giarrizzo, H.A. Bullen, T.M. Hoehler, H.A. Barton, Bacterial calcium carbonate precipitation in cave environments: a function of calcium homeostasis, Geomicrobiol. J. 27 (2010) 444–454.
[26] Hai-Bo Jiang, H.-M.C, Kun-Shan Gao, Bao-Sheng Qiu, *Inactivation of Ca^{2+}/H^{+} Exchanger in Synechocystis sp. Strain PCC 6803 promotes cyanobacterial calcification by upregulating CO_2-Concentrating mechanisms*, Appl. Environ. Microbiol. 79 (13) (2013) 4048–4055.
[27] S. Anderson, A.V, J. Huang, T. Viswanatha, A novel role for calcite in calcium homeostasis, FEBS Lett. 308 (1) (1992) 94–96.
[28] X. Li, et al., Spatial patterns of carbonate biomineralization in biofilms, Appl. Environ. Microbiol. (2015) p. AEM. 01585-15.
[29] A. Aggarwal, et al., Recurrent Pseudomonas aortic root abscess complicating mitral valve endocarditis, Heart Lung 41 (2) (2012) 181–183.
[30] T.A. Bicanic, S.J. Eykyn, Hospital-acquired, native valve endocarditis caused by Pseudomonas aeruginosa, J. Infect. 44 (2) (2002) 137–139.
[31] J. Lam, et al., Production of mucoid microcolonies by Pseudomonas aeruginosa within infected lungs in cystic fibrosis, Infect. Immun. 28 (2) (1980) 546–556.
[32] G. Skjak-Braek, E. Murano, S. Paoletti, Alginate as immobilization material. II: determination of polyphenol contaminants by fluorescence spectroscopy, and evaluation of methods for their removal, Biotechnol. Bioeng. 33 (1) (1989) 90–94.
[33] A.J. Jesaitis, et al., Compromised host defense on Pseudomonas aeruginosa biofilms: characterization of neutrophil and biofilm interactions, J. Immunol. (Baltimore, Md.) 171 (8) (2003) 4329–4339.
[34] G.J. Meluleni, et al., Mucoid Pseudomonas aeruginosa growing in a biofilm in vitro are killed by opsonic antibodies to the mucoid exopolysaccharide capsule but not by antibodies produced during chronic lung infection in cystic fibrosis patients, J. Immunol. (Baltimore, Md.) 155 (4) (1995) 2029–2038.
[35] S. Cantet, et al., Cytological characterization of apatitic calcium phosphate structures in bronchial epithelial tissue cultured from a child with cystic fibrosis (deltaF508), Virchows Arch. 439 (5) (2001) 683–690.
[36] G. Ogrinc, B. Kampalath, J.F. Tomashefski Jr., Destruction and loss of bronchial cartilage in cystic fibrosis, Hum. Pathol. 29 (1) (1998) 65–73.
[37] K.H. Hsu, et al., Pseudomonas aeruginosa endocarditis associated with endophthalmitis caused by arteriovenous fistula and graft infection, J. Chin. Med. Assoc. 66 (10) (2003) 617–620.
[38] W.B. Bean, M.C. Schmidt, Rupture of the aortic valve; disappearing diastolic pressure as a diagnostic sign, J. Am. Med. Assoc. 153 (3) (1953) 214–215.
[39] R.M. Hodges, R.R. De Alvarez, Puerperal septicemia and endocarditis caused by Pseudomonas aeruginosa, JAMA 173 (1960) 1081–1088.
[40] K.S. Smith, J.G. Ferry, Prokaryotic carbonic anhydrases, FEMS Microbiol. Rev. 24 (4) (2000) 335–366.
[41] B. Gaume, et al., Biomineralization markers during early shell formation in the European abalone Haliotis tuberculata, Linnaeus, Mar. Biol. 158 (2) (2011) 341–353.
[42] H. Tohse, H. Ando, Y. Mugiya, Biochemical properties and immunohistochemical localization of carbonic anhydrase in the sacculus of the inner ear in the salmon Oncorhynchus masou, Comp. Biochem. Physiol. Part A Mol. Integr. Physiol. 137 (1) (2004) 87–94.
[43] A. Moya, et al., Carbonic anhydrase in the scleractinian coral Stylophora pistillata: characterization, localization, and role in biomineralization, J. Biol. Chem. 283 (2008) 25475–25484.
[44] N. Favre, M.L. Christ, A.C. Pierre, Biocatalytic capture of CO2 with carbonic anhydrase and its transformation to solid carbonate, J. Mol. Catal. B Enzym. 60 (3–4) (2009) 163–170.
[45] Wei Li, L.-P.L, Peng-Peng Zhou, Long Cao, Long-Jiang Yu, Shi-Yun Jiang, Calcite precipitation induced by bacteria and bacterially produced carbonic anhydrase, Curr. Sci. 100 (4) (2011).
[46] R. Ramanan, et al., Bio-sequestration of carbon dioxide using carbonic anhydrase enzyme purified from Citrobacter freundii, World J. Microbiol. Biotechnol. 25 (6) (2009) 981–987.
[47] S.R. Lotlikar, et al., Three functional β-carbonic anhydrases in Pseudomonas aeruginosa PAO1: role in survival in ambient air, Microbiology 159 (Pt 8) (2013) 1748–1759.
[48] A.B. Murray, et al., Structural mapping of anion inhibitors to beta-Carbonic Anhydrase psCA3 from Pseudomonas aeruginosa, ChemMedChem 13 (19) (2018) 2024–2029.
[49] M.A. Pinard, et al., Structure and inhibition studies of a type II beta-carbonic anhydrase psCA3 from Pseudomonas aeruginosa, Bioorg. Med. Chem. 23 (15) (2015) 4831–4838.
[50] S. Sarkisova, et al., Calcium-induced virulence factors associated with the extracellular matrix of mucoid Pseudomonas aeruginosa biofilms, J. Bacteriol. 187 (13) (2005) 4327–4337.
[51] J. Sambrook, D.W. Russell, Molecular Cloning: a Laboratory Manual, 3rd ed., Cold Spring Harbor Laboratory Press, Cold Spring Harbor, N.Y, 2001.
[52] T.T. Hoang, et al., A broad-host-range Flp-FRT recombination system for site-specific excision of chromosomally-located DNA sequences: application for isolation of unmarked Pseudomonas aeruginosa mutants, Gene 212 (1) (1998) 77–86.
[53] K.-H. Choi, H. Schweizer, An improved method for rapid generation of unmarked Pseudomonas aeruginosa deletion mutants, BMC Microbiol. 5 (1) (2005) 30.
[54] H.P. Schweizer, T.T. Hoang, An improved system for gene replacement and xylE fusion analysis in Pseudomonas aeruginosa, Gene 158 (1) (1995) 15–22.
[55] D.G. Gibson, et al., Enzymatic assembly of DNA molecules up to several hundred kilobases, Nat Meth 6 (5) (2009) 343–345.
[56] A. Hernandez-Santana, et al., New approaches in the detection of calcium-containing microcrystals in synovial fluid, Bioanalysis 3 (10) (2011) 1085–1091.
[57] J.F. Huggett, et al., The digital MIQE guidelines: minimum information for publication of quantitative digital PCR experiments, Clin. Chem. 59 (6) (2013) 892–902.
[58] S. Rozen, H. Skaletsky, Primer3 on the WWW for general users and for biologist programmers, Methods Mol. Biol. (Clifton, N.J.) 132 (2000) 365–386.
[59] J. Ye, et al., Primer-BLAST: a tool to design target-specific primers for polymerase chain reaction, BMC Bioinformatics 13 (2012).
[60] H. Savli, et al., Expression stability of six housekeeping genes: a proposal for resistance gene quantification studies of Pseudomonas aeruginosa by real-time quantitative RT-PCR, J. Med. Microbiol. 52 (5) (2003) 403–408.
[61] A.P. Lenz, et al., Localized gene expression in Pseudomonas aeruginosa Biofilms, Appl. Environ. Microbiol. 74 (14) (2008) 4463–4471.
[62] T.D. Schmittgen, K.J. Livak, Analyzing real-time PCR data by the comparative C-T method, Nat. Protoc. 3 (6) (2008) 1101–1108.
[63] S.R. Lotlikar, et al., Three functional beta-carbonic anhydrases in Pseudomonas aeruginosa PAO1: role in survival in ambient air, Microbiology 159 (Pt 8) (2013) 1748–1759.
[64] R.G. Khalifah, The carbon dioxide hydration activity of carbonic anhydrase I. Stop-flow kinetic studies on the native human isoenzymes B and C, J. Biol. Chem. 246 (8) (1971) 2561–2573.
[65] V. Menchise, et al., Carbonic anhydrase inhibitors: stacking with Phe131 determines active site binding region of inhibitors as exemplified by the X-ray crystal structure of a membrane-impermeant antitumor sulfonamide complexed with isozyme II, J. Med. Chem. 48 (18) (2005) 5721–5727.
[66] C.T. Supuran, et al., Carbonic anhydrase inhibitors—part 52. Metal complexes of heterocyclic sulfonamides: a new class of strong topical intraocular pressure-lowering agents in rabbits, Eur. J. Med. Chem. 33 (4) (1998) 247–254.
[67] V. Garaj, et al., Carbonic anhydrase inhibitors: novel sulfonamides incorporating 1, 3, 5-triazine moieties as inhibitors of the cytosolic and tumour-associated carbonic anhydrase isozymes I, II and IX, Bioorg. Med. Chem. Lett. 15 (12) (2005) 3102–3108.
[68] M. Şentürk, et al., In vitro inhibition of human carbonic anhydrase I and II isozymes with natural phenolic compounds, Chem. Biol. Drug Des. 77 (6) (2011) 494–499.
[69] N. Krall, et al., A small-molecule drug conjugate for the treatment of carbonic anhydrase IX expressing tumors, Angew. Chemie Int. Ed. 53 (16) (2014) 4231–4235.
[70] S.U. Rehman, et al., In-vitro antibacterial, antifungal and cytotoxic activities of some coumarins and their metal complexes, J. Enzyme Inhib. Med. Chem. 20 (4) (2005) 333–340.
[71] B.W. Clare, C.T. Supuran, Carbonic anhydrase activators. 3: Structure-activity correlations for a series of isozyme II activators, J. Pharm. Sci. 83 (6) (1994) 768–773.
[72] P. Emsley, K. Cowtan, Coot: model-building tools for molecular graphics, Acta Crystallogr. D Biol. Crystallogr. 60 (12) (2004) 2126–2132.
[73] N. Ramarao, C. Nielsen-Leroux, D. Lereclus, The insect Galleria mellonella as a powerful infection model to investigate bacterial pathogenesis, J. Vis. Exp. JoVE (70) (2012).
[75] S. Sarkisova, et al., Calcium-induced virulence factors associated with the extracellular matrix of mucoid Pseudomonas aeruginosa biofilms, J. Bacteriol. 187 (13) (2005) 4327–4337.
[76] M. Aggarwal, et al., Carbon dioxide “trapped” in a β-carbonic anhydrase, Biochemistry 54 (43) (2015) 6631–6638.
[77] P. Anbu, et al., Formations of calcium carbonate minerals by bacteria and its multiple applications, Springerplus 5 (1) (2016) 250.

[78] E. Boquet, A. Boronat, A. Ramos-Cormenzana, Production of calcite (calcium carbonate) crystals by soil bacteria is a general phenomenon, Nature 246 (5434) (1973) 527.
[79] Y. Bai, et al., Experimental and visual research on the microbial induced carbonate precipitation by Pseudomonas aeruginosa, AMB Express 7 (1) (2017) 57.
[80] T.E. Bergdale, et al., Engineered biosealant strains producing inorganic and organic biopolymers, J. Biotechnol. 161 (3) (2012) 181–189.
[81] C.T. Supuran, Carbonic Anhydrases and Metabolism, Multidisciplinary Digital Publishing Institute, 2018.
[82] C. Merlin, et al., Why is carbonic anhydrase essential to Escherichia coli? J. Bacteriol. 185 (21) (2003) 6415–6424.
[83] M.I. Lorin, P.F. Gaerlan, I.D. Mandel, C.R. Denning, Composition of nasal secretion in patients with cystic fibrosis, J. Lab. Clin. Med. 88 (1976) 114–117.
[84] N.N. Sanders, H. Franckx, K. De Boeck, J. Haustraete, S.C. De Smedt, J. Demeester, Role of magnesium in the failure of rhDNase therapy in patients with cystic fibrosis, Thorax 61 (2006) 962–966.
[85] D.J. Smith, G.J. Anderson, S.C. Bell, D.W. Reid, Elevated metal concentrations in the CF airway correlate with cellular injury and disease severity, J. Cyst. Fibros. 13 (2014) 289–295.
[86] G.S. Reusz, et al., Urinary calcium and oxalate excretion in children, Pediatr. Nephrol. 9 (1) (1995) 39–44.
[87] A. Rajendra, et al., Severe hypercalcemia in a patient with pulmonary tuberculosis, J. Family Med. Prim. Care 5 (2) (2016) 509.
[88] J. Felce, M.H. Saier Jr., Carbonic anhydrases fused to anion transporters of the SulP family: evidence for a novel type of bicarbonate transporter, J. Mol. Microbiol. Biotechnol. 8 (3) (2004) 169–176.
[89] M.B. Guilloton, et al., Carbonic anhydrase in Escherichia coli. A product of the cyn operon, J. Biol. Chem. 267 (6) (1992) 3731–3734.
[90] M.B. Guilloton, et al., A physiological role for cyanate-induced carbonic anhydrase in Escherichia coli, J. Bacteriol. 175 (5) (1993) 1443–1451.
[91] G. Amoroso, et al., The gene NCE103 (YNL036w) from Saccharomyces cerevisiae encodes a functional carbonic anhydrase and its transcription is regulated by the concentration of inorganic carbon in the medium, Mol. Microbiol. 56 (2) (2005) 549–558.
[92] K.J. Thomas, C.V. Rice, Revised model of calcium and magnesium binding to the bacterial cell wall, Biometals 27 (6) (2014) 1361–1370.
[93] E. Bäuerlein, Biomineralization of unicellular organisms: an unusual membrane biochemistry for the production of inorganic nano- and microstructures, Angew. Chemie Int. Ed. 42 (2003) 614–641.
[94] R. Ramanan, et al., Bio-sequestration of carbon dioxide using carbonic anhydrase enzyme purified from Citrobacter freundii, World J. Microbiol. Biotechnol. 25 (6) (2009) 981–987.
[95] R. Yadav, et al., Single enzyme nanoparticle for biomimetic CO 2 sequestration, J. Nanoparticle Res. 13 (1) (2011) 263–271.
[96] M.P. Kennedy, et al., Calcium stone lithoptysis in primary ciliary dyskinesia, Respir. Med. 101 (1) (2007) 76–83.
[97] S.M. Katz, L.J. Krueger, B. Falkner, Microscopic nephrocalcinosis in cystic fibrosis, N. Engl. J. Med. 319 (5) (1988) 263–266.
[98] D. Poller, et al., Bacterial calcification in infective endocarditis, Postgrad. Med. J. 65 (767) (1989) 665–667.
[99] N. Morris, D. Stickler, R. McLean, The development of bacterial biofilms on indwelling urethral catheters, World J. Urol. 17 (6) (1999) 345–350.
[100] R. SAMMONS, et al., Bacterial calcification: friend or foe? Nano Biomed. 2 (2) (2010) 71–80.
[101] J.M. Connolly, et al., Estimation of a biofilm-specific reaction rate: kinetics of bacterial urea hydrolysis in a biofilm, NPJ Biofilms Microbiomes 1 (2015) 15014.
[102] T. Alelign, B. Petros, Kidney stone disease: an update on current concepts, Adv. Urol. 2018 (2018).
[103] S. Alok, et al., Pathophysiology of kidney, gallbladder and urinary stones treatment with herbal and allopathic medicine: a review, Asian Pac. J. Trop. Dis. 3 (6) (2013) 496.
[104] V.Y. Bird, et al., Pseudomonas aeruginosa as an etiologic agent of nephrolithiasis in deep water divers, J. Endourol. Case Rep. 3 (1) (2017) 4–6.
[105] S. Geider, et al., Calcium carbonate crystals promote calcium oxalate crystallization by heterogeneous or epitaxial nucleation: possible involvement in the control of urinary lithogenesis, Calcif. Tissue Int. 59 (1) (1996) 33–37.
[106] S.A. Sarkisova, et al., A Pseudomonas aeruginosa EF-hand protein, EfhP (PA4107), modulates stress responses and virulence at high calcium concentration, PLoS One 9 (6) (2014) p. e98985.
[107] M.S. Son, et al., In vivo evidence of Pseudomonas aeruginosa nutrient acquisition and pathogenesis in the lungs of cystic fibrosis patients, Infect. Immun. 75 (11) (2007) 5313–5324.
[108] P. Bielecki, et al., Ex vivo transcriptional profiling reveals a common set of genes important for the adaptation of Pseudomonas aeruginosa to chronically infected host sites, Environ. Microbiol. 15 (2) (2013) 570–587.
[109] K.S. Smith, et al., Carbonic anhydrase is an ancient enzyme widespread in prokaryotes, Proc. Natl. Acad. Sci. 96 (26) (1999) 15184–15189.
[110] R.H. Valdivia, S. Falkow, Fluorescence-based isolation of bacterial genes expressed within host cells, Science (New York, N.Y) 277 (5334) (1997) 2007–2011.
[111] I. Nishimori, et al., Inhibition studies of the β-carbonic anhydrases from the bacterial pathogen Salmonella enterica serovar Typhimurium with sulfonamides and sulfamates, Bioorg. Med. Chem. 19 (16) (2011) 5023–5030.
[112] A.S. Covarrubias, et al., Structure and function of carbonic anhydrases from Mycobacterium tuberculosis, J. Biol. Chem. 280 (19) (2005) 18782–18789.
[113] J. Rengarajan, B.R. Bloom, E.J. Rubin, Genome-wide requirements for Mycobacterium tuberculosis adaptation and survival in macrophages, Proc. Natl. Acad. Sci. 102 (23) (2005) 8327–8332.
[114] B.K. Johnson, et al., The carbonic anhydrase inhibitor ethoxzolamide inhibits the Mycobacterium tuberculosis PhoPR regulon, Esx-1 secretion and attenuates virulence, Antimicrob. Agents Chemother. (2015) p. AAC. 00719-15.
[115] P. Burghout, et al., Inhibition of the β-carbonic anhydrase from Streptococcus pneumoniae by inorganic anions and small molecules: toward innovative drug design of antiinfectives? Bioorg. Med. Chem. 19 (1) (2011) 243–248.
[116] T. Klengel, et al., Fungal adenylyl cyclase integrates CO2 sensing with cAMP signaling and virulence, Curr. Biol. 15 (22) (2005) 2021–2026.
[117] I. Nishimori, et al., Carbonic anhydrase inhibitors: the β-carbonic anhydrase from Helicobacter pylori is a new target for sulfonamide and sulfamate inhibitors, Bioorg. Med. Chem. Lett. 17 (13) (2007) 3585–3594.
[118] I. Nishimori, et al., Carbonic anhydrase inhibitors: DNA cloning and inhibition studies of the α-carbonic anhydrase from Helicobacter pylori, a new target for developing sulfonamide and sulfamate gastric drugs, J. Med. Chem. 49 (6) (2006) 2117–2126.
[119] S. Bury-Mone, et al., Roles of alpha and beta carbonic anhydrases of Helicobacter pylori in the urease-dependent response to acidity and in colonization of the murine gastric mucosa, Infect. Immun. 76 (2) (2008) 497–509.
[120] P. Joseph, et al., A new β-carbonic anhydrase from Brucella suis, its cloning, characterization, and inhibition with sulfonamides and sulfamates, leading to impaired pathogen growth, Bioorg. Med. Chem. 19 (3) (2011) 1172–1178.
[121] E. Pérez, et al., An essential role for phoP in Mycobacterium tuberculosis virulence, Mol. Microbiol. 41 (1) (2001) 179–187.
[122] T. Minakuchi, et al., Molecular cloning, characterization, and inhibition studies of the Rv1284 β-carbonic anhydrase from Mycobacterium tuberculosis with sulfonamides and a sulfamate, J. Med. Chem. 52 (8) (2009) 2226–2232.
[123] R.P. Henry, G.A. Kormanik, Carbonic anhydrase activity and calcium deposition during the molt cycle of the blue crab Callinectes sapidus, J. Crustacean Biol. 5 (2) (1985) 234–241.
[124] W.E. Müller, et al., Induction of carbonic anhydrase in SaOS-2 cells, exposed to bicarbonate and consequences for calcium phosphate crystal formation, Biomaterials 34 (34) (2013) 8671–8680.
[126] B.W. Holloway, V.K, A.F. Morgan, Chromosomal genetics of Pseudomonas, Microbiol. Mol. Biol. Rev. 43 (1) (1979) 73–102.